LABORATORY INVESTIGATIONS OF THE PHOTOCHEMICAL DEGRADATION OF ACETALDEHYDE (CH$_3$CHO) AND ACRYLIC ACID (CH$_2$CHCOOH) IN ICE

BY

BENJAMIN EDUAFO SAMPSON

MASTER THESIS

SUBMITTED IN PARTIAL FULFILMENT OF THE REQUIREMENTS FOR THE DEGREE OF MASTER OF SCIENCE IN ENVIRONMENTAL PHYSICS

UNIVERSITY OF BREMEN

JULY 2010

Laboratory investigations of the photochemical degradation of acetaldehyde (CH$_3$CHO) and acrylic acid (CH$_2$CHCOOH) in ice

by

Benjamin Eduafo Sampson

FIRST REFEREE**:** **Prof. Dr. Otto Schrems**

SECOND REFEREE**:** **PD. Dr.Annette Ladstätter-Weißenmayer**

Declaration

I herewith declare that I did the written work on my own and only with the means as indicated.

……………………………………………

Date and signature

Acknowledgement

Dedication

This work is dedicated to my parents for their love and financial support throughout my stay and studies in Bremen, Germany.

Abstract

The uptake and incorporation of atmospheric trace gases in water ice, their interactions and chemical reactions with water molecules provides an understanding of processes at the ice/air interface. Solar irradiance can consequently trigger photochemical reactions of these atmospheric trace gases in snow and on ice surfaces resulting in the formation of trace gases such as oxidized nitrogen, halogen species, hydrogen peroxide etc. These species can be released into the overlying atmosphere and perturb the gas phase chemistry. The combination of cryogenic spectroscopy (matrix isolation technique) together with Fourier Transform infrared spectroscopy (FTIR) detection method is a unique experimental method for studying reactions of this type in the laboratory. It has been used to monitor the photodecomposition of two atmospheric carbonyl compounds (CH_3CHO and $CH_2CHCOOH$) trapped in H_2O ice and in solid rare gases. The results show that photochemistry in snow or ice destroys organic molecules and produces smaller molecules such as CO, CO_2 etc.

Contents

Chapter 1: Introduction

Chapter 2: Theoretical Background of the experimental work

Chapter 3: Experimental work and results

Chapter 4: Summary and Conclusions

References

List of figures

Chapter 1: Introduction

1.1 General Introduction

Ice in the environment either in the form of ice particles, clouds, sea ice, glaciers or snow at the Earth's surface has an influence on the atmosphere's composition and the climate system. In recent years, the interaction between the atmosphere and the cryosphere has received growing attention. Knowledge of the exchange between the atmosphere and the underlying snowpack is important for the development of transfer functions that link concentrations in snowpack. 50 % of land is covered by snow or ice in the northern hemisphere which is seasonal dependent while a part of the world's polar oceans is covered by sea ice. Rather than being inert, snow or ice covered regions of the Earth can be sinks or sources of atmospheric trace gases as well as possible chemical processes on the ice surface or in the bulk ice. Snow can also be a reactive matrix for trapped atmospheric trace gases. Photoproducts formed in the snowpack by photolysis with sunlight can either be released into the boundary layer or trapped in the ice. Research on snowpack processes and atmosphere-snow gas exchange has demonstrated that chemical and physical interactions between the snowpack and the overlying atmosphere have a substantial impact on the composition of the lower atmosphere. The interaction of trace gases and ice surfaces has an impact in the interpretation of ice core records and modeling of chemical processes taking place in the atmosphere. The atmospheric composition in polar regions is strongly influenced by the interaction of trace gases with the sea ice and snow/firn surfaces. On the other hand ice particles in clouds play an important role in the stratospheric ozone depletion (PSCs) and in the chemistry of the upper troposphere (cirrus clouds). **[1, 2, 3]**

1.2 Components of the climate system

The climate system can be best described as a dynamic system which is in a transient equilibrium most times. The influence of the various external forcing mechanisms, most important of which is the sun, internal dynamics and interactions introduce changes in the climate system. The temperature difference caused by differential heating of the sun induce motion in the atmosphere (wind) and ocean (current) which transport energy from the warm

tropics to the cold poles. This transport is controlled by many interactions within the climate system (see fig. 1). The climate system consists of four major components: the atmosphere, the cryosphere, the lithosphere and the biosphere. **[4]**
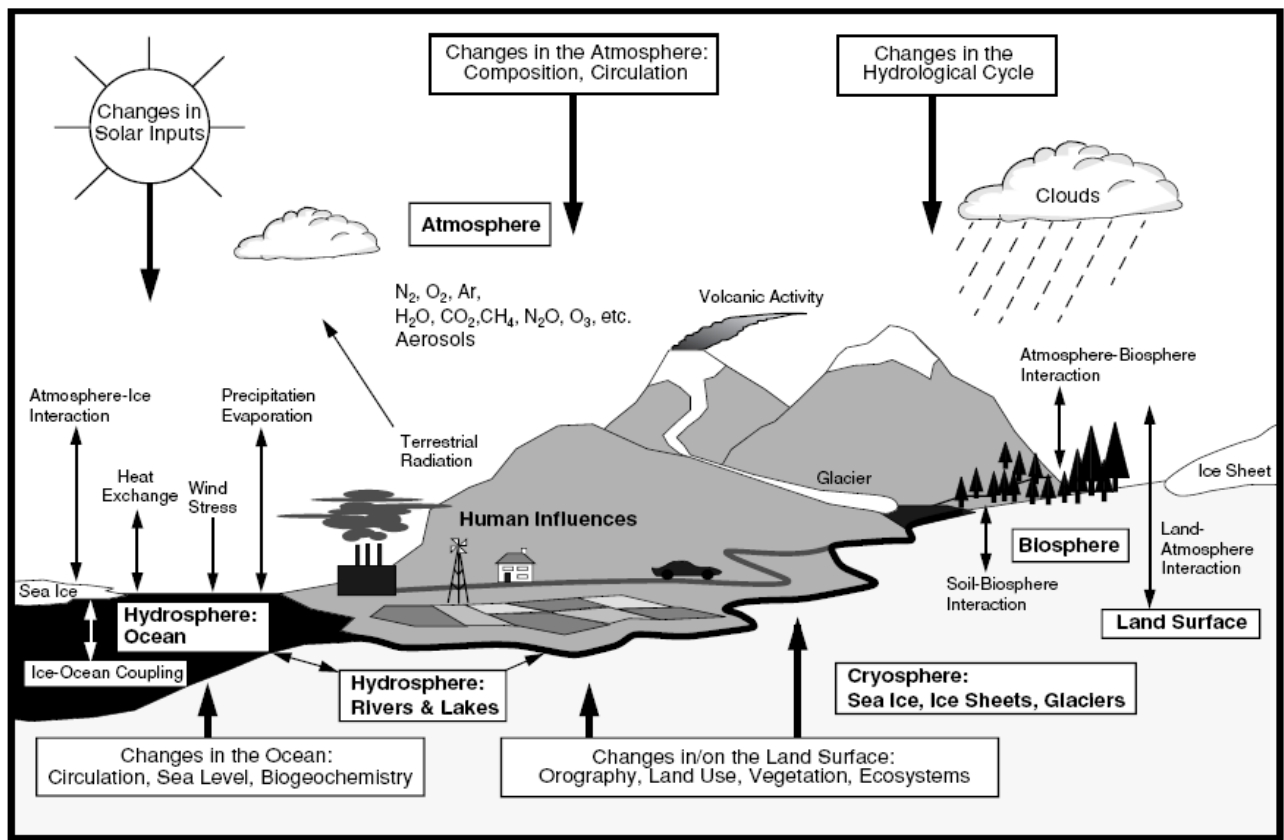
Fig.1 Schematic view of the component of the global climate system (Bold), their processes and interactions (thin arrows) and some aspects that may change (Bold arrows). **[Source: ref. 5]**

1.2.1   The atmosphere

The Earth's atmosphere is basically a thin layer of gases that surrounds the Earth. It is a binary system consisting of dry air and water vapour. It is the most unstable and rapidly changing part of the system which has its composition changed with the evolution of the Earth.

The atmosphere influences the climate system through radiative, chemical and dynamical processes which are all interconnected. It consists of three components:

1. A gas mixture (78% Nitrogen, 21% Oxygen and 1% water vapour, Carbon dioxide, Ozone and other trace gases.
2. Water vapour and ice particles which appear as clouds (Cirrus clouds) and precipitation (rain, snow, hail etc).
3. Suspended particles called aerosols (soot, dust etc).

The pressure of the atmosphere is highest at the surface and decreases with height because air at the surface is compressed by the weight of all the air above it. At higher levels, the weight of the air above is smaller and less compression leading to lower pressure. Based on temperature, the atmosphere is divided into four layers: the Troposphere, Stratosphere, Mesosphere and Thermosphere (see fig. 2). The troposphere ranges from the ground level to about 10km. It is where temperature decreases with height at an average rate of 6.4 °C for every 1km increase in height. This decrease in temperature is caused by adiabatic cooling (as air rises, the atmospheric pressure reduces so the air expands doing work on the surroundings and therefore reducing the temperature). Most of the mass of the atmosphere (75-80%) is in this region. Almost all weather occurs within this layer. The transition boundary between the troposphere and the above layer is called the tropopause. The stratosphere is where temperature increases with height due to the absorption of ultraviolet radiation from the sun by ozone. The vertical stratification, with warmer layers above and cooler layers below, makes the stratosphere dynamically stable. There is no regular convection and associated turbulence in this part of the atmosphere. About 90% of the ozone in the atmosphere is found in this layer. The stratopause is the transition layer between the stratosphere and the layer above. The mesosphere, where temperature decreases with height down to -80 °C occupies the region 50 – 80km above the surface of the Earth. Most meteors from space burn in this layer. The transition boundary between the mesosphere and the layer above is the mesopause. The thermosphere is where temperature increases significantly to about 1200 °C at an altitude of 500km. it is the biggest of all the layers of the Earth's atmosphere. Air is really thin in this layer. **[4,6]**
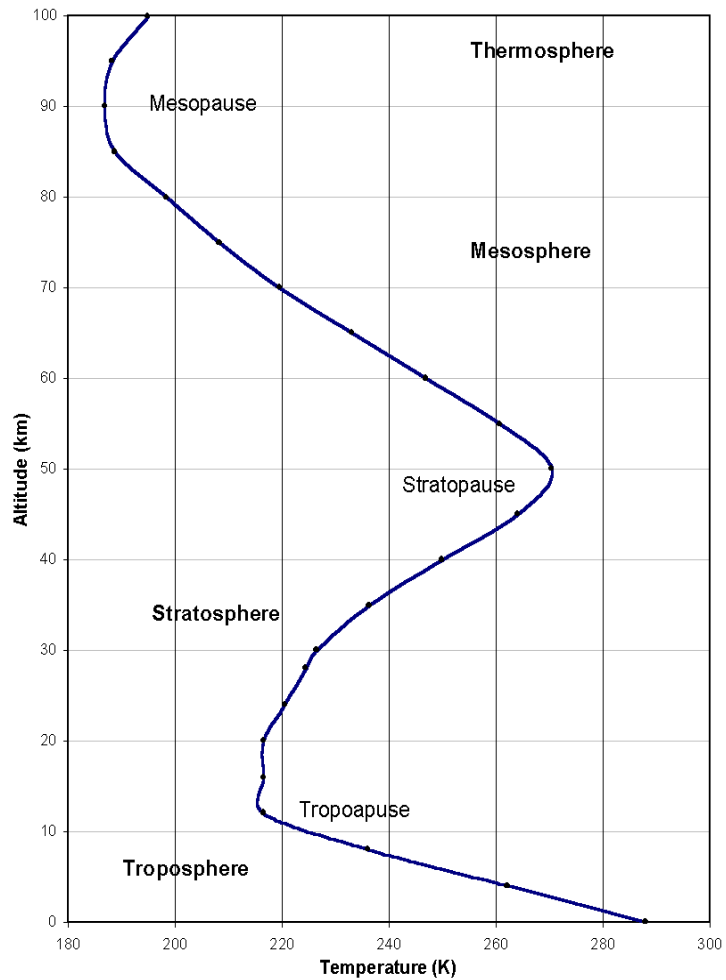
Fig.2 A view of the structure of the atmosphere **[source: ref. 7]**

1.2.2   The hydrosphere

It comprises all liquid surfaces including oceans, rivers, lakes and aquifers, fresh water etc. About 70% the Earth's surface is covered by liquid surfaces (oceans). The ocean can be described as a binary system consisting of water and salt. Oceanic motion is driven at the surface and changes of the oceanic state are a response to local forcing (heating, cooling, precipitation, evaporation etc.) and to advection of horizontal gradients of velocity, temperature and salinity. The hydrosphere influence the climate system through the storage and transportation of heat /energy, source and sink of large quantities of trace gases and regulation of the hydrological cycle. **[4,5]**

1.2.3 The cryosphere

The cryosphere consist of snow, sea ice, ice shelves and ice sheets. It is the second largest in terms of mass and heat capacity of the components of the climate system (after the ocean). Interactions between the cryosphere and the climate include, temperature – ice – albedo feedback, cooling of the atmosphere above snow and ice surfaces, snow and ice acting as effective insulators, melting of sea ice and ice sheets thereby stabilizing the oceanic stratification and obstruction of atmospheric circulation like mountains. The role of the cryosphere on the climate system includes, surface energy balance, impact on gas exchange between the atmosphere and Earth surface, impacts on water supply and water cycle and impact on sea level (ice mass imbalance). **[4,5]**

1.2.4 The lithosphere

The lithosphere consists of the continents and ocean floor. It may be considered as a constant boundary condition for atmosphere and ocean on short time scales and on longer time scales, the continental drift leads changes of the distribution of continents and ocean floor. The lithosphere influences the climate system through changes in the rate and pattern of the mantle's flow leading to changes in the rate of CO_2 degassing and its release into the atmosphere. It also affects atmospheric and oceanic circulation by the distribution of continents (mountains, passages etc). the eruption of volcanoes lead to the ejection of particulate matter and sulphate bearing gases, forming aerosols which affect the radiation balance of the atmosphere and climate. **[4,5]**

1.2.5 The biosphere

The biosphere consists of living organisms (biota) and dead organic matter. It controls how energy received from the sun is returned to the atmosphere. It has a major impact on the atmosphere's composition. The biota influence the uptake and release of greenhouse gases. The biosphere plays a major role in the carbon cycle on Earth, as well as in the budgets of trace gases such as methane and nitrous oxide. Other biospheric emissions are the volatile organic compounds (VOC) which may have effects on atmospheric chemistry, aerosol formation and on climate. Biotic indicators such as tree rings, pollens, fossils and other records which provide

information about past climate are preserved as a result of the influence of climate on the biosphere. **[5]**

1.3 Water molecule and the nature of ice surfaces

Water (H_2O) is the most abundant compound on the Earth's surface constituting about 70% of the planet's surface. In nature it exists in liquid, solid and gaseous states. The hydrogen bonds in its condensed form are extremely important in determining its physical and chemical properties. Most of the volume of water molecules are these bonds which result from the small size of the hydrogen atoms in comparison to the large size of oxygen atoms (see fig.3). Each oxygen atom has three electron pairs in its electron cloud, one of which it shares with two hydrogen atoms forming covalent bonds in the water molecules. The two hydrogen atoms form weak hydrogen bonds with oxygen of adjacent water molecules (see fig. 3). These bonds are responsible for water's ability to store large amounts of heat energy with relatively small temperature changes. **[6]** Water in the solid phase exhibits one of the most complex phase diagrams having about sixteen or so crystalline phases (where the oxygen atoms are in fixed positions relative to each other but the hydrogen atoms may or may not be disordered but obeying the 'ice rule') and three amorphous (non crystalline) phases. Hexagonal ice or I_h is one of the many crystalline phases of ice and is the form of all natural snow and ice on earth and is of interest in the study of snow photochemistry since it possesses many peculiar properties relevant to the existence of life and regulation of global climate. **[8]**

Snow/ice forms either by condensation of water vapour onto an ice forming nucleus or by the freezing of supercooled droplets. Ice is one of the most widespread natural material, its unusual mechanical, electrical, thermal and especially surface properties determine various aspects of our everyday life. On the Earth surface, ice exist in the form of snow (precipitation in the of crystalline water ice), glaciers, sea ice, ice sheets etc. In the atmosphere, ice can be found in the upper troposphere in the form of cirrus clouds and condensation trails (contrails) from airplanes, Polar stratospheric clouds (PSCs) in the stratosphere and polar mesospheric clouds in the mesosphere which consist of ice crystals. Water molecules in ice (I_h) are held together by hydrogen bonds. The oxygen atoms form six sided rings arranged in layers with each layer is the mirror image of adjacent ones (see fig.4).
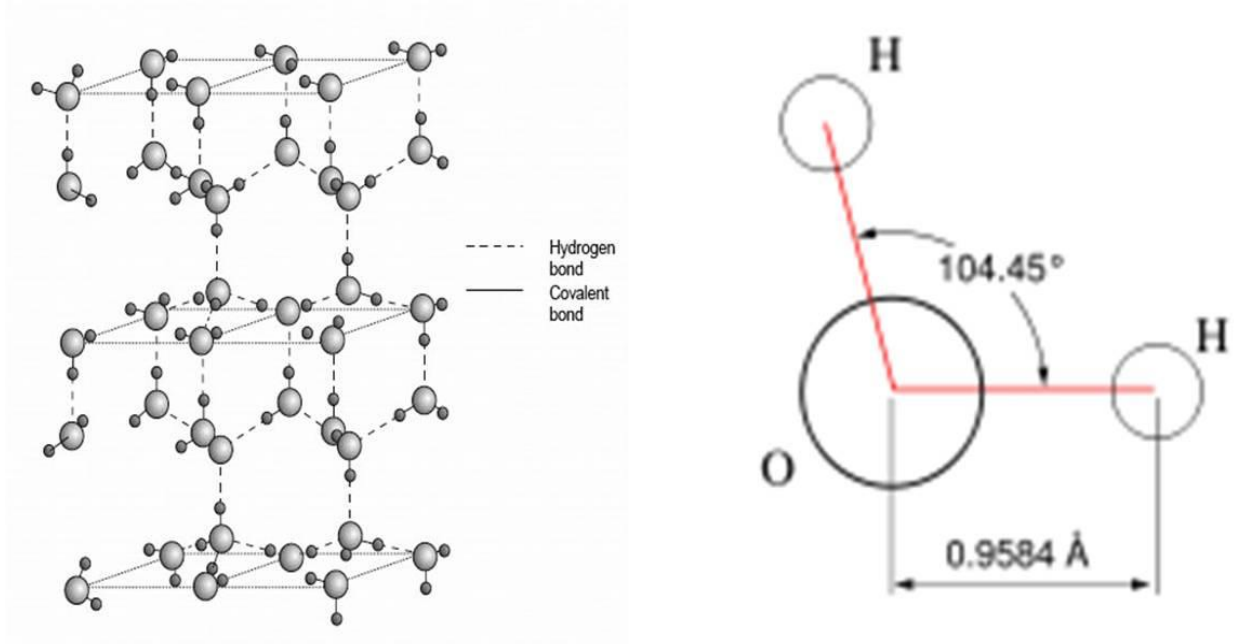
Fig.3 Schematic representation of water molecule (right) and ice lattice showing the hydrogen and covalent bonds (left). **[Source: ref. 9]**
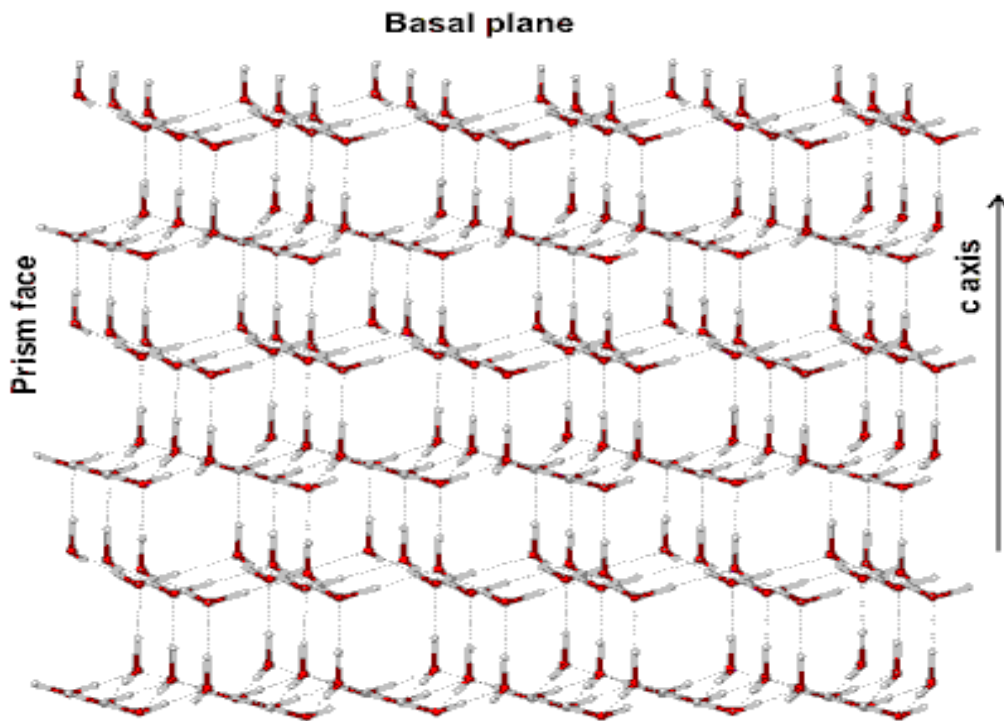
Fig.4 A sketch of the molecular structure of hexagonal ice (I_h). **[Source: ref. 9]**

The result is a fairly open network which gives ice a lower density than that of liquid water because the molecules in ice are not so tightly packed as in liquid water.
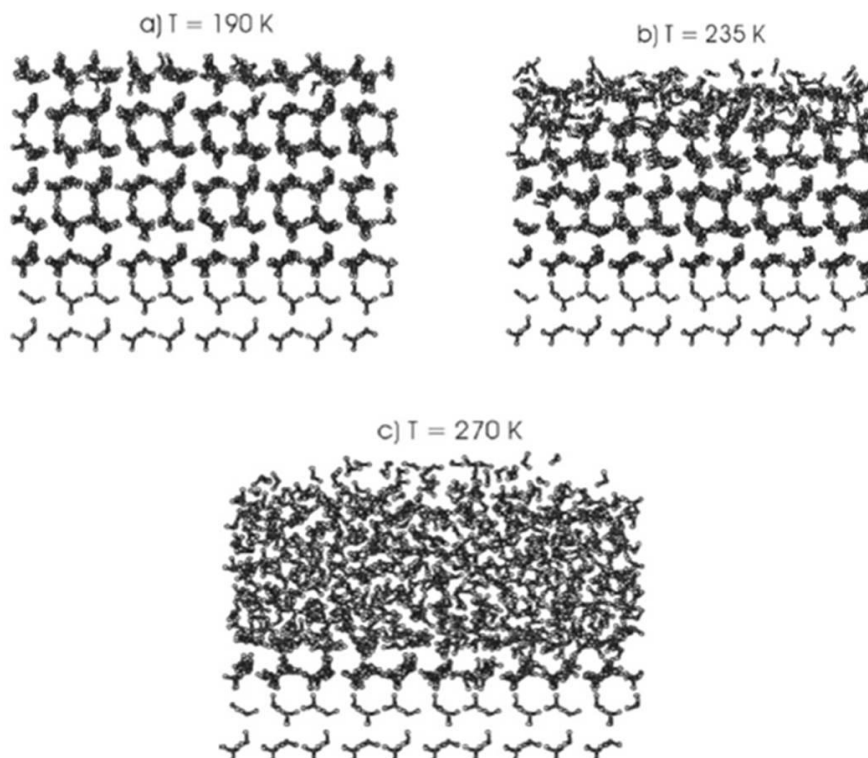
Fig.5 A sketch showing a molecular dynamics study of surface premelting on hexagonal ice **[Source: ref. 10]**

There are difficulties in understanding and characterizing reactions in snow and on ice surfaces which are enhanced by insufficient knowledge of the physical and chemical nature of natural ice surfaces. A disordered layer, often called the quasi liquid layer (QLL) exists on ice surfaces. The existence of the QLL at temperatures close to the ice melting point was investigated by Faraday in the middle of the 19th century. It exists over a wide range of environment, from the depths of glaciers to stratospheric ice clouds and also known to be of vital importance in ozone depletion. The thickness of the QLL increases with temperature and ionic solute concentration. Its thickness is present at a state where the free energy of the ice system is at a minimum and is governed by the competition between the free energy of the ice surface and the energy required to melt a solid layer. Its properties are intermediate between those of bulk ice and liquid water, complicating efforts to elucidate the reaction kinetics in the medium. In addition, it affects chemical reactions in the upper atmosphere because it changes the way molecules stick to the surface of the ice

(i.e. absorption onto and dissolution into the QLL). Figure 5 shows a molecular dynamic simulation of the surface disorder with temperature. At low temperature, only the upper most ice layer deviates from the ideal hexagonal ice lattice, both the intensity and the depth of the disordered region increases with increasing temperature.

The IR spectrum of H_2O ice at a temperature of 20 K is shown in figure 6. The O-H stretching vibrations of H_2O ice appears around $3000 - 3500cm^{-1}$ and the O-H deformation modes appears around $1600cm^{-1}$.
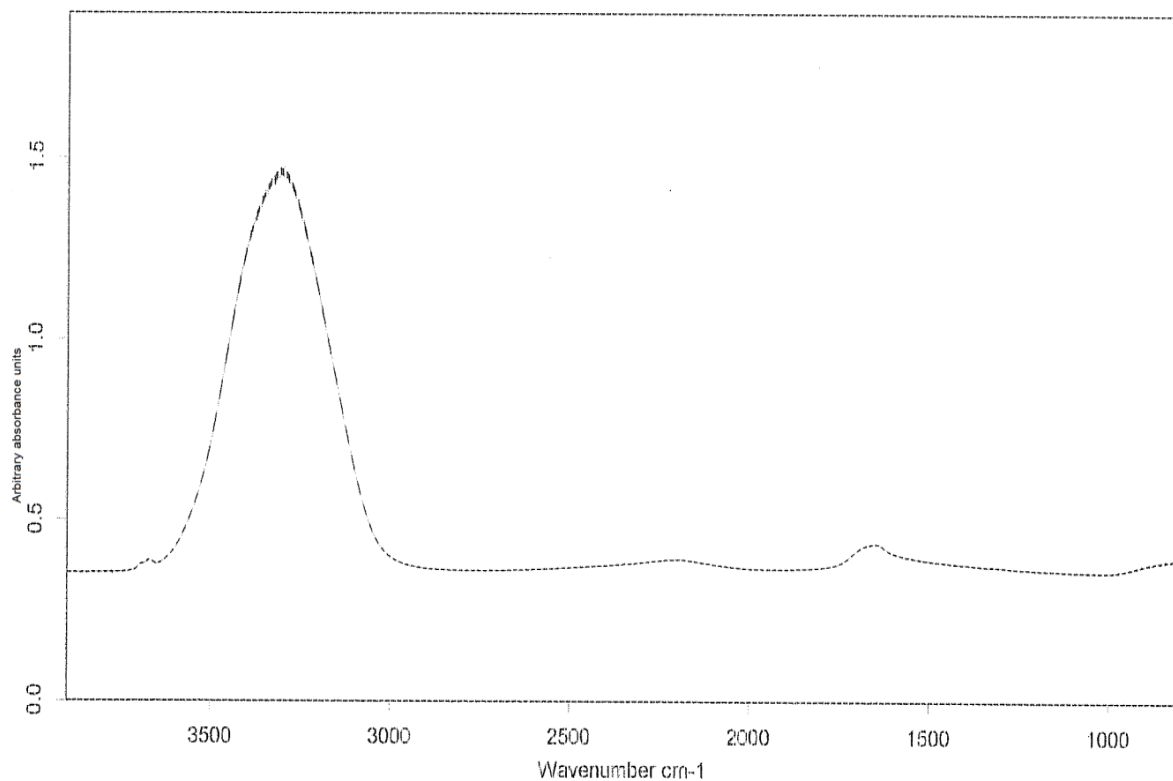
Fig.6 IR spectrum of H_2O ice at T = 20 K

1.4 Photochemical processes in ice

The science of snow and ice photochemistry is a relatively young, interdisciplinary field, drawing on expertise in a wide range of areas. Ice is an important component in atmospheric chemistry due to its physical and chemical properties and its occurrence in atmospheric aerosols (ice clouds). The diffusion of trapped trace gases in an ice matrix is slow and the solubility is low. The bulk contribution is less important than the surface adsorption.
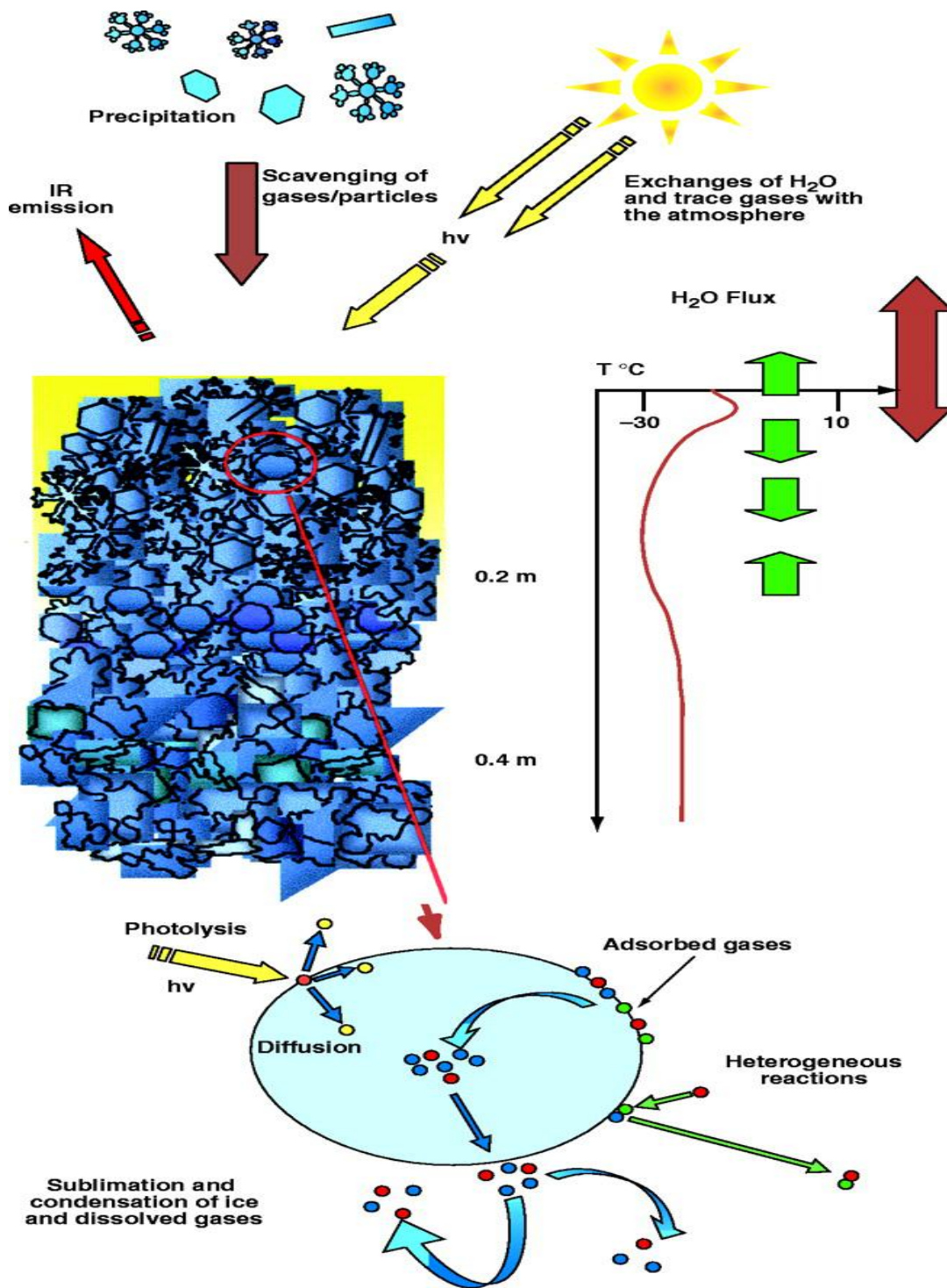
Fig.7 Physical and chemical processes involved in the air-snow interactions **[source: ref. 11]**

Molecules hitting the ice surface will either be reflected back to the gas phase or be accommodated on the surface into different types of adsorption states**. [10]**

Photochemical reactions i.e. reactions induced by ultraviolet radiation (UV) and visible light play a major role in the environment. Photochemistry of molecules in ice or on ice surfaces is initiated mainly by UV radiation because these photons have energies high enough to break chemical bonds. These reactions on compounds in snow or on ice surfaces can have important implications for the composition of the atmospheric boundary layer in snow-covered regions and for the interpretation of concentration profiles in snow and ice regarding the composition of the past atmosphere. UV radiation of wavelengths shorter than 290 nm (UV-C region) is completely absorbed by the ozone layer in the stratosphere and not important in tropospheric chemistry. UV-B radiation (290-320 nm) partially passes through the ozone layer and is responsible for tropospheric ozone photolysis and the production of hydroxyl (OH) radicals. At high latitudes, the sun never gets as high in the sky as it does at lower latitudes. Hence, this decreases the photolysis rates with increasing latitudes. However, snow and ice surfaces have a high albedo which causes an increase of atmospheric photolysis rates. [2] Numerous physical and chemical processes affect trace gases in the snowpack.
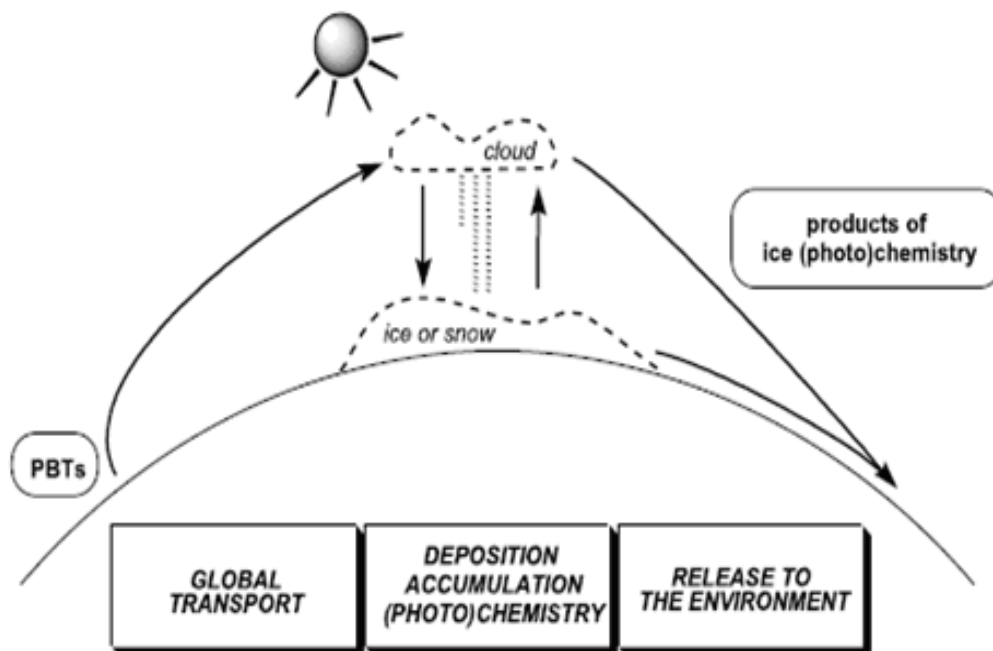
Fig. 8 Ice photochemistry and its implication on the environment. [**Source.ref 12**]

These processes include adsorption, solid state diffusion and chemical reactions catalyzed by ice surfaces that can be initiated by light or by temperature. Figure 7 illustrates possible physical and chemical processes involved in air - snow interactions. [11] Photochemical reactions of trace constituents in the snow result in the formation of gases, including oxidized nitrogen, halogen species, organic compounds and hydrogen peroxide, which subsequently are released into the atmosphere and perturb the gas-phase HOx budget. [3] For instance, Klàn and Holoubek 2002 proposed a model according to which persistent, bioaccumulative and toxic compounds (PTBs) can be generated by photochemistry of primary pollutants in natural ice and snow and subsequently released to the environment. [12] This is further illustrated in Figure 8.

1.5 Motivation

Ice, being one of the condensed phases present in the Earth's atmosphere and surface, still remains a gap in our understanding of how atmospheric trace gases interact with it. [13] Water ice plays a role in the photochemistry of species trapped in its lattice. It can modify the electronic states of the species or act as a reactive cage leading to subsequent reactions of the photofragments with the nearest water molecules. Furthermore, water ice photolysed with UV radiation below 200 nm dissociates and water photoproducts can react with the photofragments of the trapped molecules. [14]

Recent evidence shows that sunlit snow and ice play an important role in processing atmospheric species. Photochemical production of a variety of chemical species has recently been reported to occur in snow/ice and the release of these photochemically generated species may significantly impact the chemistry of the overlying atmosphere. [2]

For that reason, this work focuses on the photochemical degradation of acetaldehyde and acrylic acid trapped in water ice and the photoproducts of such species using Fourier Transform Infrared (FTIR) Spectroscopy as the detection method. Acetaldehyde is one of the atmospheric trace gases which is considered to be an atmospheric pollutant which is potentially carcinogenic and mutagenic. A major anthropogenic source is mainly by incomplete combustion of ethanol fuel used in cars. This is of particular interest as a renewable alternative to fossil fuel. It is abundant in the upper troposphere with a mixing ratio in the order of 30-100 pptv [15]. On the

other hand, acrylic acid which is one of the volatile organic acids in the atmosphere is severely irritating and aggressive to the skin and respiratory tract. It is released into the atmosphere mainly by species of algae in seawater during the breakdown of dimethyl sulphoniopropionate (DMSP) to produce dimethylsulphide (DMS) and acrylic acid. [16] This is described by the following equation:

$$(CH_3)_2S^+CH_2CH_2COO^- \longrightarrow (CH_3)_2S + CH_2CHCOOH \qquad (1.0)$$

$$\qquad \text{DMSP} \qquad\qquad\qquad \text{DMS} \qquad \text{acrylic acid}$$
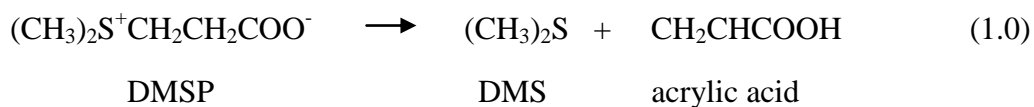
Both compounds can be precursors of cloud condensation nuclei or contribute to the formation of photochemical smog in the presence of other precursors. They are removed from the atmosphere by oxidation initiated by hydroxyl (OH) radicals, photolytic degradation and also wet or dry deposition.

1.6 Previous works

C.O. Delle Védova and O. Sala 1991, [17] have reported about the photochemical behavior of acetaldehyde isolated in solid argon and nitrogen. The photoproducts observed were CO and CH_4 in both matrices. **P.K. Hudson et al. 2002,** [**15**] reported on the interaction of methanol, acetone and acetaldehyde with ice and nitric acid doped ice and its implication on Cirrus clouds. Similar studies was reported by **M. Petit Jean et al. 2009, [18]** on the uptake of acetaldehyde on solid ice surfaces and on solid/liquid super cooled mixtures doped with nitric acid in the temperature range of 203-253K. **S. Houdier et al. 2002, [19]** measured acetaldehyde in snow and **C. Guimbaud et al. 2002, [20]** also measured acetaldehyde in the overlying air at ALERT summit (82°N, Canadian high Arctic). In a recent study, **F. Domine et al. 2010, [21]** have performed a season long study of the evolution of acetaldehyde concentrations in the subarctic snowpack near Fairbanks (65°N) central Alaska. Quite recently, **D.B. Millet et al. 2010, [22]** have reported of an investigation about the global atmospheric budget of acetaldehyde using a 3-D GEOS-Chem model. They used an ensemble of observations to evaluate present understanding of its sources and sinks**.** Many papers have reported about the ambient level measurements of acetaldehyde in cities across the world and photodissociation of acetaldehyde in the gas phase.

J. Umemura and S. Hayashi 1974, [23] studied the infrared spectra and molecular configurations of liquid and crystalline acrylic acids. A similar study was reported by **M. Orgill et al. 1999, [24]** about FTIR studies of conformational isomerism in acrylates and acrylic acids. **A. Kulbida et al. 1995, [25]** have reported investigations of rotational isomerism in acrylic acid, which included a combined matrix-isolation infrared, Raman and ab initio molecular orbital study. **R.N. Rosenfeld and B. Weiner 1983, [26]** studied the photo dissociation dynamics of acrylic acid at 248nm and 193nm using an infrared fluorescence technique and concluded that decarboxylation is the major pathway at both wavelengths. **M.C. Osbourne et al. 1999, [27]** reported results of a flash photolysis study on acrylic acid and measured the relative yields of the major products such as HOCO, CO_2 and CO with the infrared diode laser absorption technique. A similar study was conducted by **Wei-Hai Fung and Ruo-Zhuang Lin 2000, [28]** using time-resolved infrared absorption using tunable, narrow band diode lasers.

Chapter 2:   Theoretical background of the experimental work

2.1 Infrared Spectroscopy

Infrared spectroscopy has been a technique for material analysis in the laboratory for many decades. It is one of the most common spectroscopic techniques used by organic and inorganic chemists. Simply, infrared radiation is passed through a sample, some of it is absorbed and some passed through (transmitted). Absorption in the infrared region results in changes in vibrational and rotational status of the molecule. In most instances, the infrared spectrum is a unique molecular fingerprint of the molecule under investigation that is easily distinguished from the absorption pattern of other molecules.

2.2 Infrared frequency range

The infrared region of the electromagnetic spectrum ranges from 13000-10 cm^{-1}. This region is commonly divided into three areas, notably near infrared, mid infrared and far infrared. The near infrared or overtone region (13000-4000 cm^{-1}) needs minimal or no sample preparation. It offers high-speed quantitative analysis without consumption or destruction of the sample. The region of most interest for chemical analysis is the mid-infrared region (4000-400 cm^{-1}) which corresponds to the fundamental vibrations of molecules. The far infrared region (400-10 cm^{-1}) is useful for molecules containing heavy atoms such as inorganic compounds but rather requires specialized experimental techniques. A view of the electromagnetic spectrum and the infrared region are shown in figures 9 and 10.

Infrared radiation is measured in wavenumber ν (cm^{-1}) or wavelength λ (μm) units. The wavenumber is directly proportional to frequency and the energy of infrared absorption.

$$\nu = \upsilon c \qquad\qquad E = \frac{h\upsilon}{c} \qquad\qquad (2.1)$$

Where c = velocity of light, E= energy, h= Planck's constant, υ= frequency.

Information from an infrared absorption spectrum is presented in plots as wavenumber or wavelength versus the absorption intensity or percentage transmission.
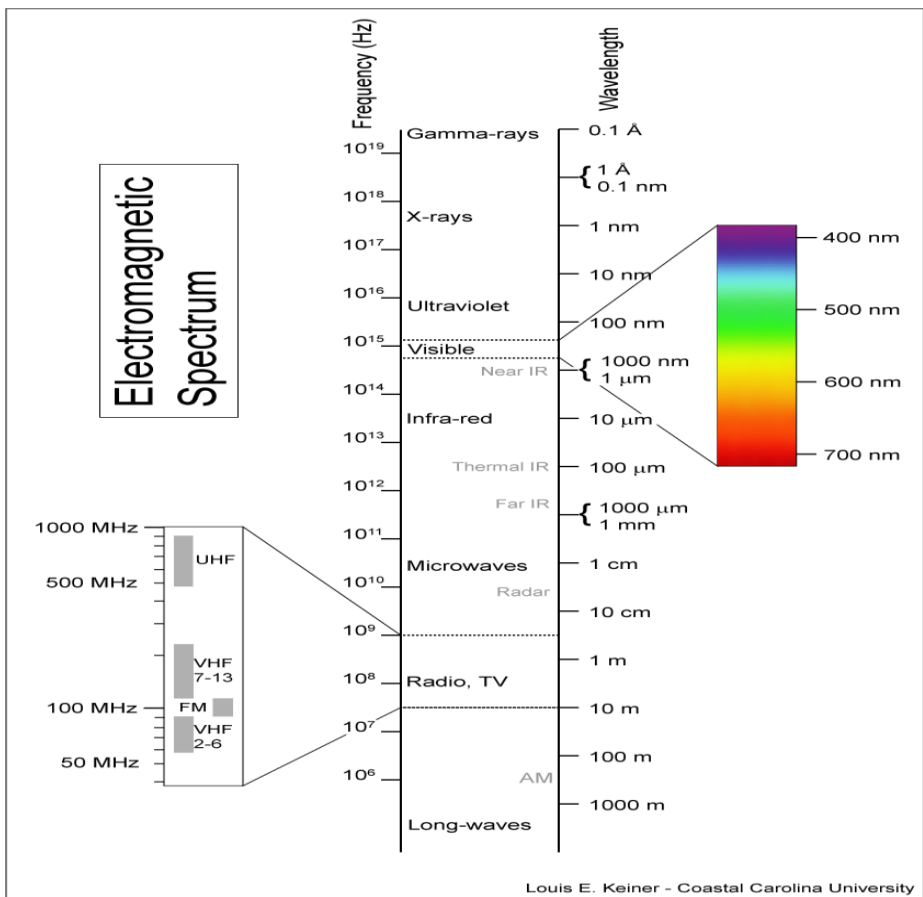
Fig. 9 A view of the electromagnetic spectrum **[source: ref. 29]**
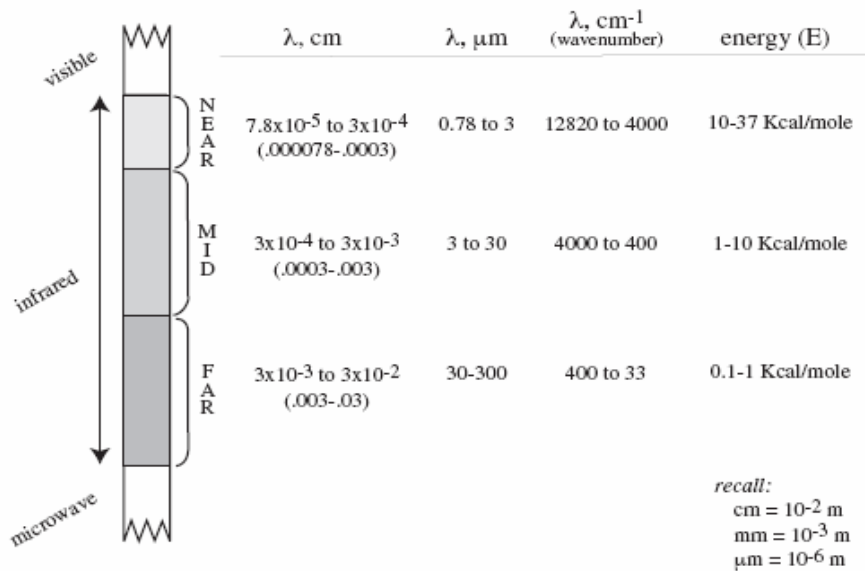
Fig. 10 Infrared region of the electromagnetic spectrum **[source: ref. 30]**

Transmittance (T) represents the ratio of radiant power transmitted by a sample (I) to the radiant power incident on the sample (I_o).

$$T = \frac{I}{I_o} \tag{2.2}$$

Absorbance (A) represents a measure of the quantity of light that a sample neither transmits nor reflects. It is proportional to the concentration of a substance or the logarithm to the base 10 of reciprocal of transmittance (T).

$$A = \log_{10}\left[\frac{1}{T}\right] \quad = \quad -\log_{10} T \quad = \quad -\log_{10} \frac{I}{I_o} \tag{2.3}$$

The absorbance is linear with the concentration (or number density of absorbers) and is described by Lambert-Beer's law:

$$A = \varepsilon \, L \, C = \alpha \, L \tag{2.4}$$

Where ε = molar absorptivity, L = path length, C = concentration of absorbing species α = absorption coefficient of the substance. Hence,

$$T = \frac{I}{I_o} \quad = 10^{-\varepsilon LC} \tag{2.5}$$

Transmittance spectra provide better contrast between intensities of strong and weak bonds because transmittance ranges from 0 to 100% whereby absorbance ranges from zero to infinity.

2.3 Principles of molecular spectroscopy

In general, molecules cannot exist in all energy states but rather they have series of discrete values. The energy levels of a molecule are divided into rotational, vibrational, electronic and translational energy states **[31].**

$$\text{i.e} \quad E_{total} = E_{vib} + E_{rot} + E_{elec} + E_{trans} \tag{2.6}$$

The translational energy is related to the displacement in space as a function of normal thermal motion of matter. The electronic energy is related o the electronic movement in the potential due to arrangement of protons and neutrons in the nucleus and it is dependent on the distance between the atomic nuclei. Electronic transitions occur in the ultraviolet and visible regions of

the electromagnetic radiation (wavelength range: 100nm – 1000nm). The vibrational energy corresponds to absorption of energy by a molecule as the component atoms vibrate about the mean centre of their chemical bonds. This transitions occurs in the infra red region (wavelength = 10μm). Rotational energy is associated with transitions in the microwave region (wavelength = 1cm). A molecule in an excited vibrational state will have rotational energy and can lose energy in a transition which alters both the vibrational and rotational energy content of the molecule. The total energy of a molecule in a specific vibrational and rotational state denoted by the pair of quantum numbers (v, J), can be written as:

$$E\ (v,\ J) = E_{vib}\ (v) + E_{rot}\ (J) \tag{2.7}$$

2.3.1 Vibrational energy of a diatomic molecule

Transitions in the vibrational energy levels are a result of absorption of radiation whereby the energy of the radiation exactly matches the difference in energy levels between the vibrational quantum states which will result in a change in the dipole moment. The simplest model to describe the vibrational motion is a harmonic oscillator. i.e. The nuclei are connected by a spring (see fig. 11).
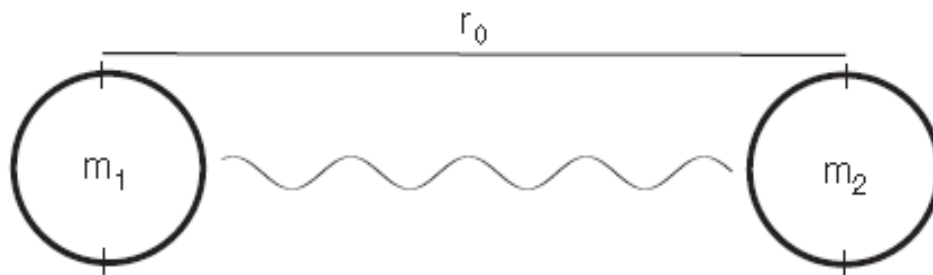
Fig. 11 Model of a simple harmonic oscillator [32]

When the nuclei are displaced from their equilibrium positions, they experience a restoring force F, which is proportional to the displacement $(r-r_o)$ according to Hooke's law with k as the restoring force constant.

$$F = -k(r-r_o) \tag{2.8}$$

The restoring force F is negative since it is directed opposite to the displacement of the atoms. The vibrational frequency of such a system is given by:

$$\nu = \frac{1}{2\pi} \sqrt{\frac{k}{\mu}} \tag{2.9}$$

where μ is the reduced mass of the molecules given by :

$$\mu = \frac{M_1 M_2}{M_1 + M_2}, \tag{2.10}$$

where M_1 and M_2 are the masses of the atoms in the molecule.

The potential energy E is given by :

$$E = \frac{1}{2}k(r - r_o)^2 \tag{2.11}$$

The model implies that the potential relation is approximated by a parabola (see fig. 12)
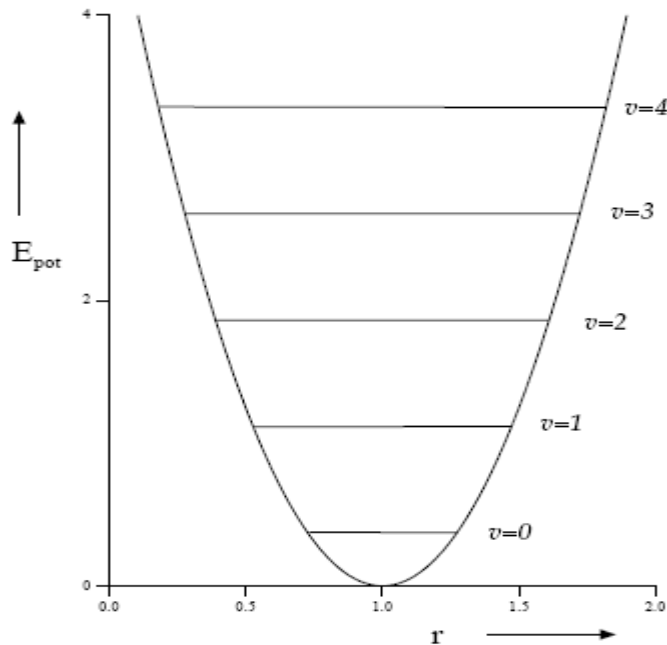
Fig. 12 Potential energy level as a function of displacement for harmonic oscillator. [33]

The vibrational energy is quantized and the allowed energies are given by :

$$E_{vib} = (v + \tfrac{1}{2})\,\hbar\omega \tag{2.12}$$

Where v is the vibrational quantum number that take values of 0, 1, 2, ... ω is the vibrational frequency.

From the vibrational energy E_{vib} (equation 2.12), the lowest energy level E_0 and the first excited state E_1 are given as :

$$E_0 = \tfrac{1}{2}\hbar\omega \quad \text{and} \quad E_1 = \tfrac{3}{2}\hbar\omega \tag{2.13}$$

Since the vibrational energy is quantized, the observed selection rule must be obeyed according to quantum mechanics. The observed transition is given by $\Delta v = \pm 1$. The transition between two states is given by :

$$E_{v+1} - E_v = (v+1+\tfrac{1}{2})\,\hbar\omega - (v+\tfrac{1}{2})\,\hbar\omega \tag{2.14}$$
$$= \hbar\omega$$

Thus, the energy difference is independent of the quantum number v, all at the same frequency. Higher transitions of $2\hbar\omega$, $3\hbar\omega$ etc (see fig.13) are sometimes observed in the energy level diagram. Such transitions result in the formation of bands called overtones.
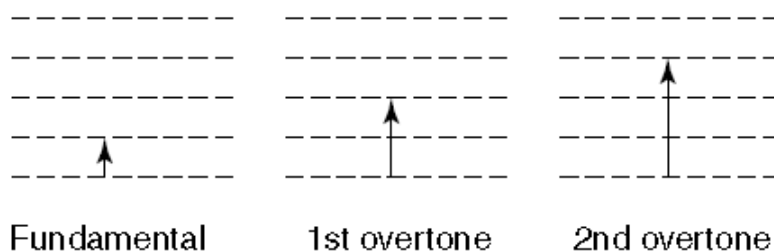
Fig. 13 Energy levels for fundamental and overtone infrared bands **[34]**

Molecules sometimes do not follow the laws of simple harmonic motion. These are described by anharmonic oscillators. This is because real bonds although elastic are not so homogeneous to obey Hooke's law (see fig. 14).

The Morse function is an expression that describes the anharmonic oscillator with the energy given as :

$$E = D_e\,(1 - \exp(-\alpha(r - r_o)))^2 \tag{2.15}$$

With D_e as dissociation energy and α is the bond constant for a particular molecule.
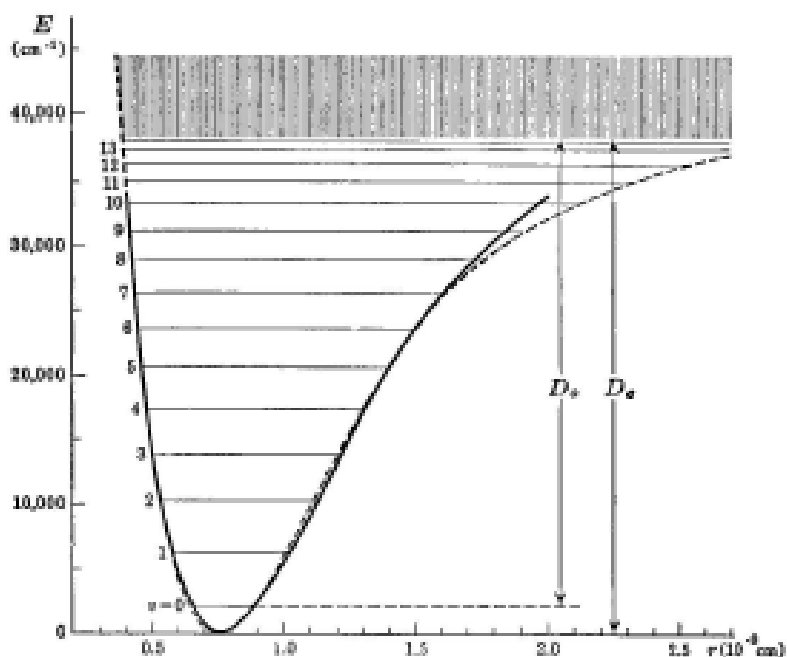
Fig. 14 Energy as a function of intermolecular distance for anharmonic oscillator. **[32]**

2.3.2 Rotational energy of a diatomic molecule

The rotational energy level within a molecule correspond to the different possible ways in which a portion of a molecule can revolve round the chemical bond that binds it to the remainder of the molecule. The rotational energy can be illustrated by a rigid rotator (see fig. 15)
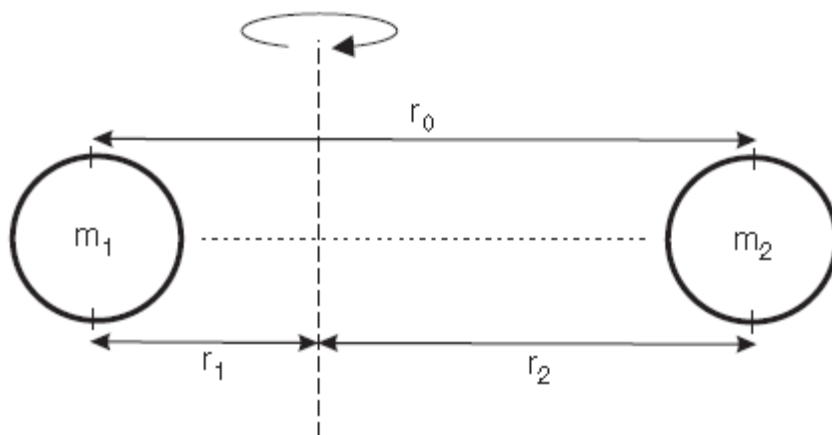
Fig.15 Model of a rigid rotator to illustrate the rotational energy of a diatomic molecule. **[32]**

With the rotational energy given by :

$$E_{rot} = \frac{1}{2}I\omega^2 = \frac{J^2}{2I} \qquad (2.16)$$

ω is the rotational freguency, I = moment of inertia of the molecule, J = angular momentum J = Iω.

From figure 15, $r_o = r_1 + r_2$ and $m_1 r_1 = m_2 r_2$. The moment of inertia $I = m_1 r_1^2 + m_2 r_2^2$

$$I = \frac{M_1 M_2}{M_1 + M_2} r_o = \mu r_o^2 \qquad (2.17)$$

Where $\mu = \frac{M_1 M_2}{M_1 + M_2} = \frac{1}{\mu} = \frac{1}{M_1} + \frac{1}{M_2}$ called the reduced mass. $\qquad (2.18)$

The angular momentum is quantized and the possible energy state is given as :

$$E_J = \frac{\hbar^2}{2I} J(J+1) \qquad (2.19)$$

J = 0, 1, 2, … is the rotational quantum number.

Expressing the energy in terms of wavenumber ($\upsilon = \frac{E}{hc}$), hence the energy :

$$E_J = \frac{\hbar}{4\pi I c} J(J+1) = BJ(J+1) \qquad (2.20)$$

Where B is the rotational constant $= \frac{\hbar}{4\pi I c} = \frac{\hbar}{4\pi \mu c r^2}$ $\qquad (2.21)$

The transition frequency is given :

$$\upsilon_{J+1 \leftarrow J} = E_J(J+1) - E_J(J)$$
$$= B(J+1)(J+2) - BJ(J+1)$$
$$= 2B(J+1) \qquad (2.22)$$

The selection for transition between rotational states is given by $\Delta J = \pm 1$ and energy diagram is illustrated in figure 16.

2.3.3 Combined rotational and vibrational transitions

Rotational – vibrational transitions can occur in the infrared wavelength region. i.e. transitions between different levels within a given electronic state. **[35]** For each electronic level, there are many vibrational levels and for any vibrational level, many rotational one (see fig. 17).

22
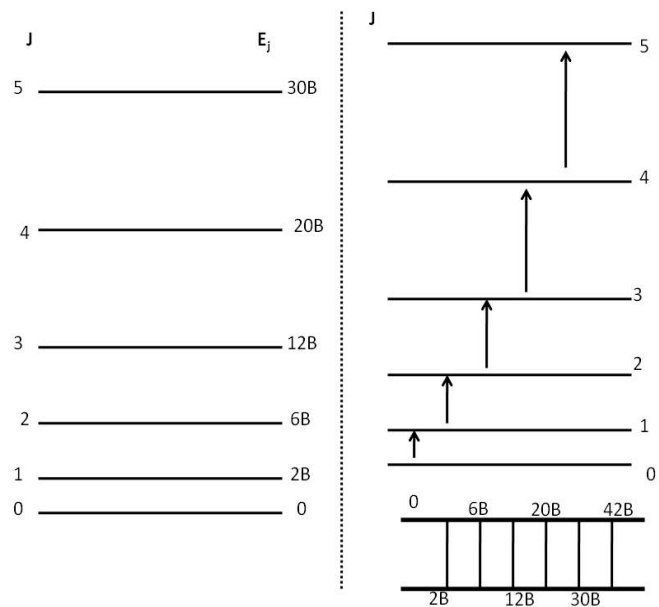
Fig.16 Rotational energy levels of a rigid diatomic molecule (left) and the allowed transitions of a rigid rotator (right). **[36]**
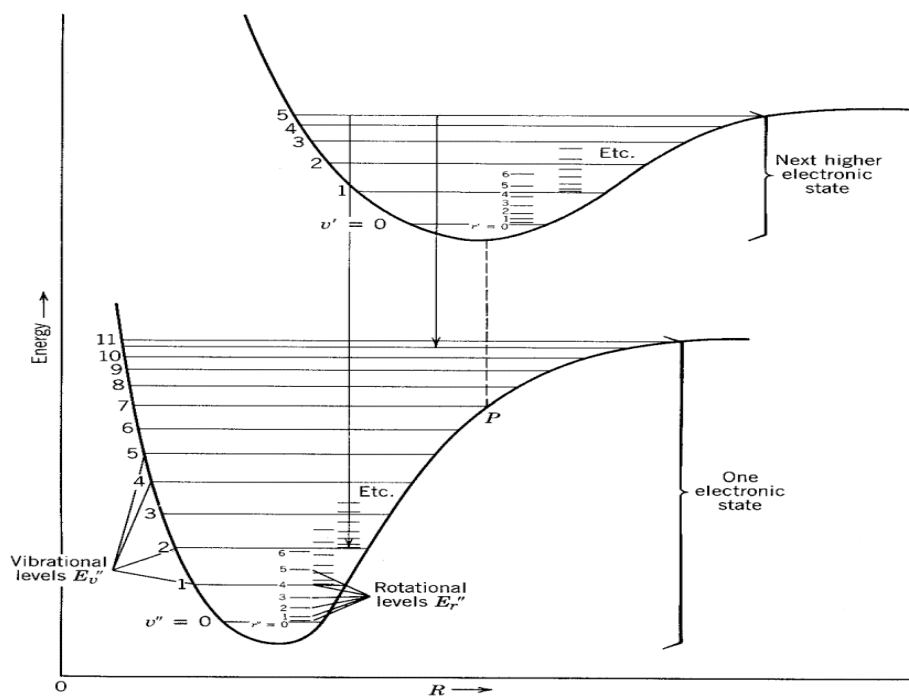
Fig.17 Molecular energy versus internuclear separation, with the various harmonic oscillator and rigid rotator states superposed. **[37]**

23

As stated earlier, the energy of a molecule in a specific vibrational and rotational state denoted by the pair of quantum numbers (v, J) is given as:

$$E_{(v, J)} = E_{vib}(v) + E_{rot}(J) \qquad (2.23)$$

The selection rule for such a combined motion is denoted by:

$$\Delta v = \pm 1, \pm 2, \pm 3 \dots \quad \text{and} \quad \Delta J = \pm 1$$

The vibrational-rotational spectrum for transitions from v = 0 and v = 1 is obtained from the relation:

$$E(v, J) = S(v+1, J'') - S(v, J') \qquad (2.24)$$

Where J' and J" are the rotational quantum numbers in states v = 1 and v = 0 respectively.

There are three transitions for v → v+1. When the rotational quantum number (J) decreases by 1 is called P – branch, those with which it (J) increases by 1 is called the R – branch and those with (J) equal to zero (0) or unchanged is called the Q – branch transitions. This is illustrated in figure 18.

2.4 Molecular vibrations

All molecules continuously vibrate even at a temperature close to absolute zero. [38] A molecule absorbs infrared radiation when the frequency of a specific vibration is equal to the frequency of the infrared radiation directed on the molecule. In general, each molecule has 3 degrees of freedom, corresponding to motions along any of the 3 Cartesian coordinate axes (x, y, and z). A polyatomic molecule of N atoms has 3N total degrees of freedom. Nonlinear molecules possess 3N-6 fundamental vibrations while linear molecules possess 3N-5 fundamental vibrations. Those that produce a net change in the dipole moment are infrared active. The major types of molecular vibrations are stretching and bending modes. Stretching is the change in interatomic distance along the bond axis. The two types of stretching vibrations are symmetric and antisymmetric modes. Bending is the change in the angle between two bonds. There are four

types of bending vibrations and they are in-plane rocking, in-plane scissoring, out-of-plane wagging and out-of-plane twisting. Figure 19 shows the various vibrations.
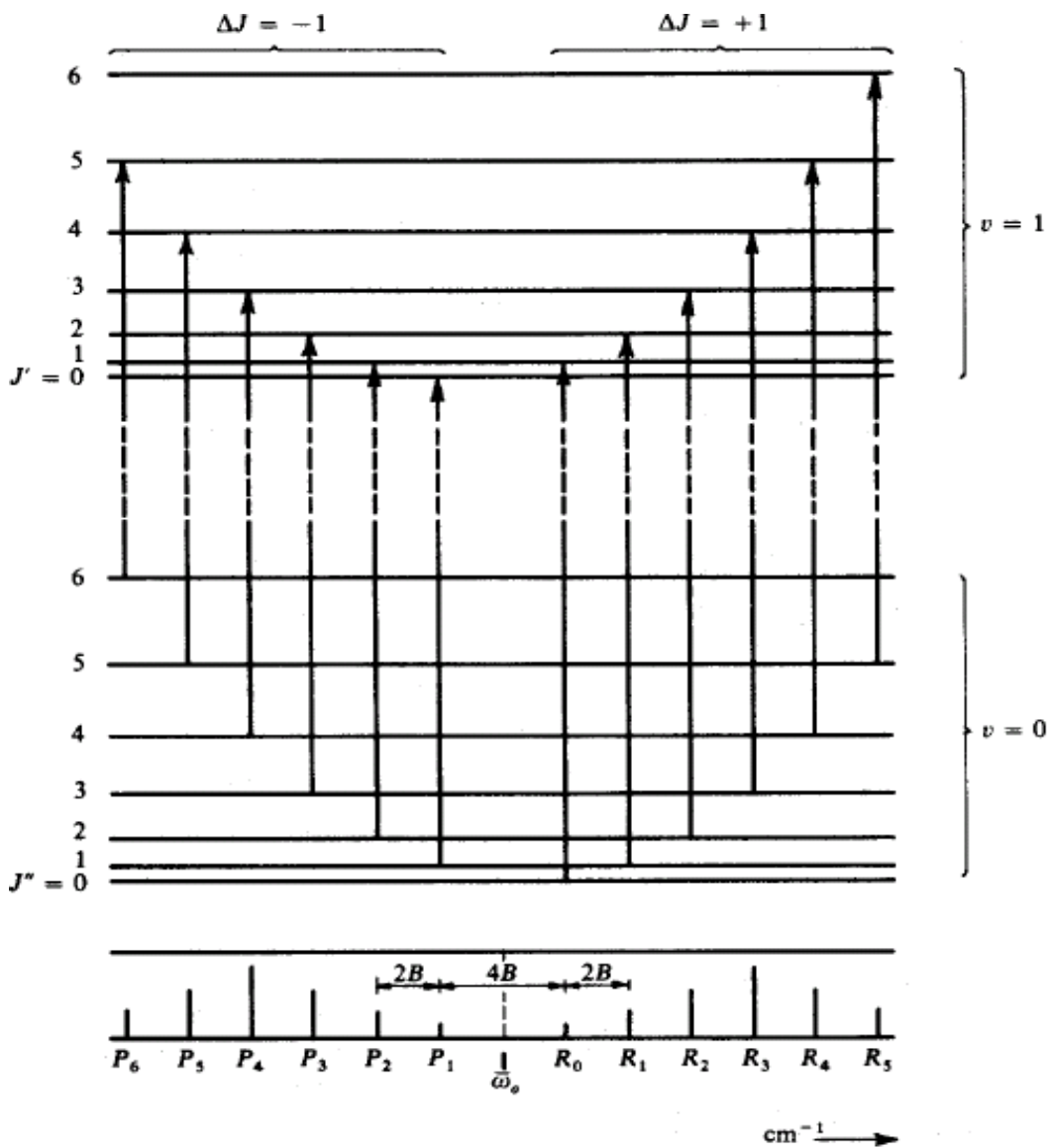
Fig.18 Sketch of the spectrum arising from some transitions between rotational-vibrational energy levels of a diatomic molecule. **[33]**

Symmetric   Asymmetric

(a) Stretching vibrations

In-plane rocking   In-plane scissoring

Out-of-plane wagging   Out-of-plane twisting

(b) Bending vibrations

© 2007 Thomson Higher Education
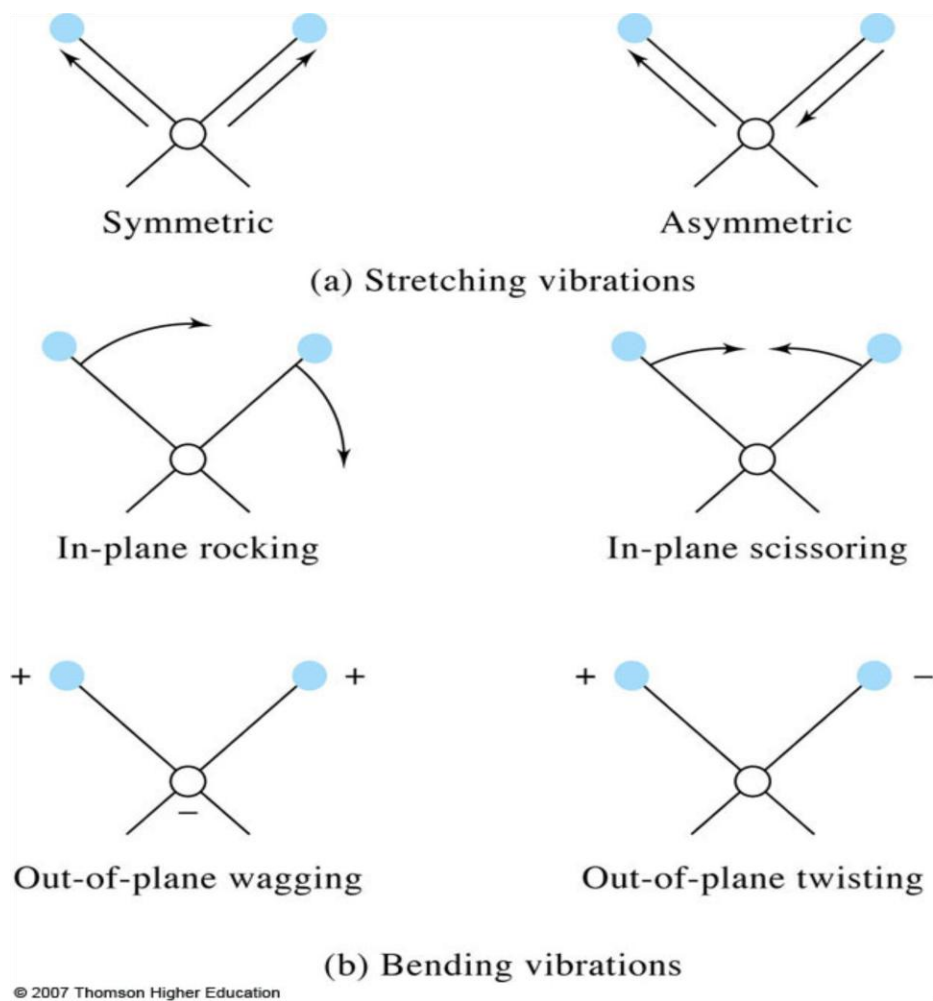
Fig.19: Illustration of stretching and bending vibrations. **[Source: ref. 39]**

2.5 Fourier Transform Infrared (FTIR) Spectroscopy

FTIR spectroscopy is a technique used to measure the absorption and emission of radiation with high precision. It can be used in remote sensing on board of satellites, on board of aircrafts and ships, at the ground and also in the laboratory. A FTIR spectrometer is based on a Michelson interferometer where one of the two mirrors is fixed and a second one moves periodically with constant velocity [see fig. 20]. The interferometer consists of these two mirrors, a detector and a beamsplitter. Radiation from the IR source is directed to the beam splitter which splits the beam into two parts. One part is reflected to the fixed mirror and the other part is transmitted to the moving mirror which moves back and forth.

26
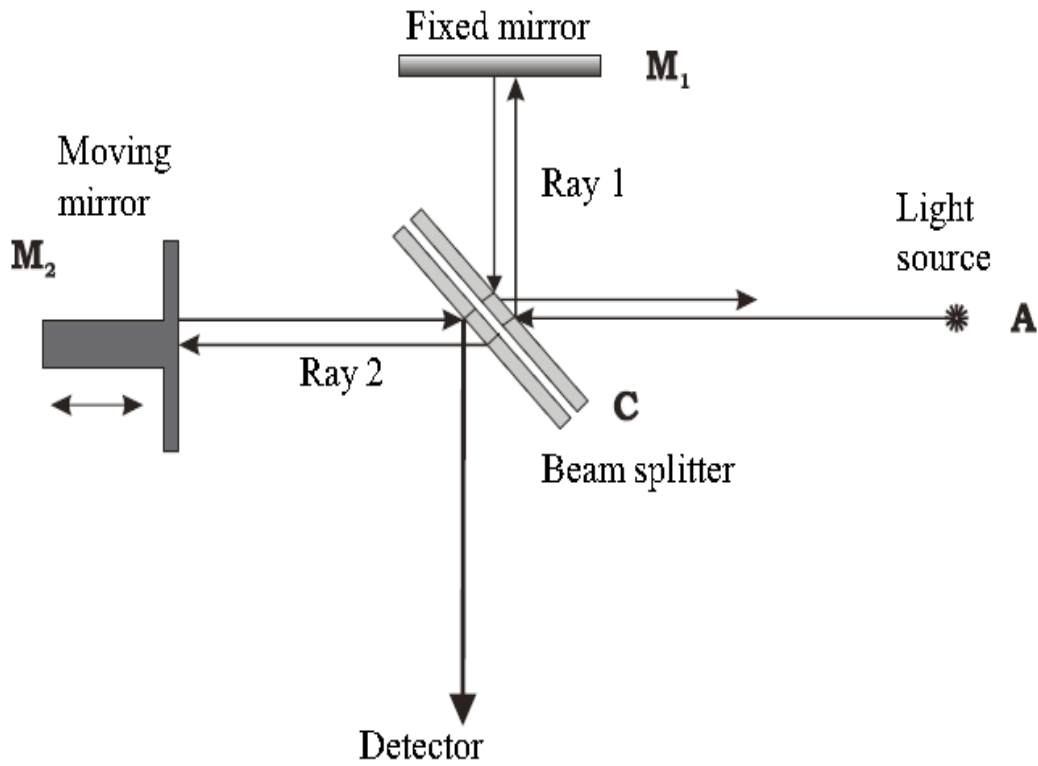
Fig.20: Schematic diagram of the Michelson Interferometer **[source: ref. 31]**

An interference pattern is created when the two beams combine. Some recombine constructively (when they arrive at the detector in phase) and some destructively (when they arrive out of phase due to the movable mirror).The interference which is called the interferogram (i.e the interference modulated signal as a function of the optical path difference) is registered at the IR detector which counts the incoming signal dependent on the optical path difference and converts it to a digital signal (Analogue-to-digital converter).

To obtain the infrared spectrum, the detector signal is sent to a computer which carries out the so-called Fourier transformation in order to convert the interferogram into a single beam spectrum (intensity as a function of wavenumber or wavelength). A reference or background single beam spectrum is collected without the sample and the sample single beam spectrum is ratioed to the background single beam spectrum to produce a transmittance spectrum.
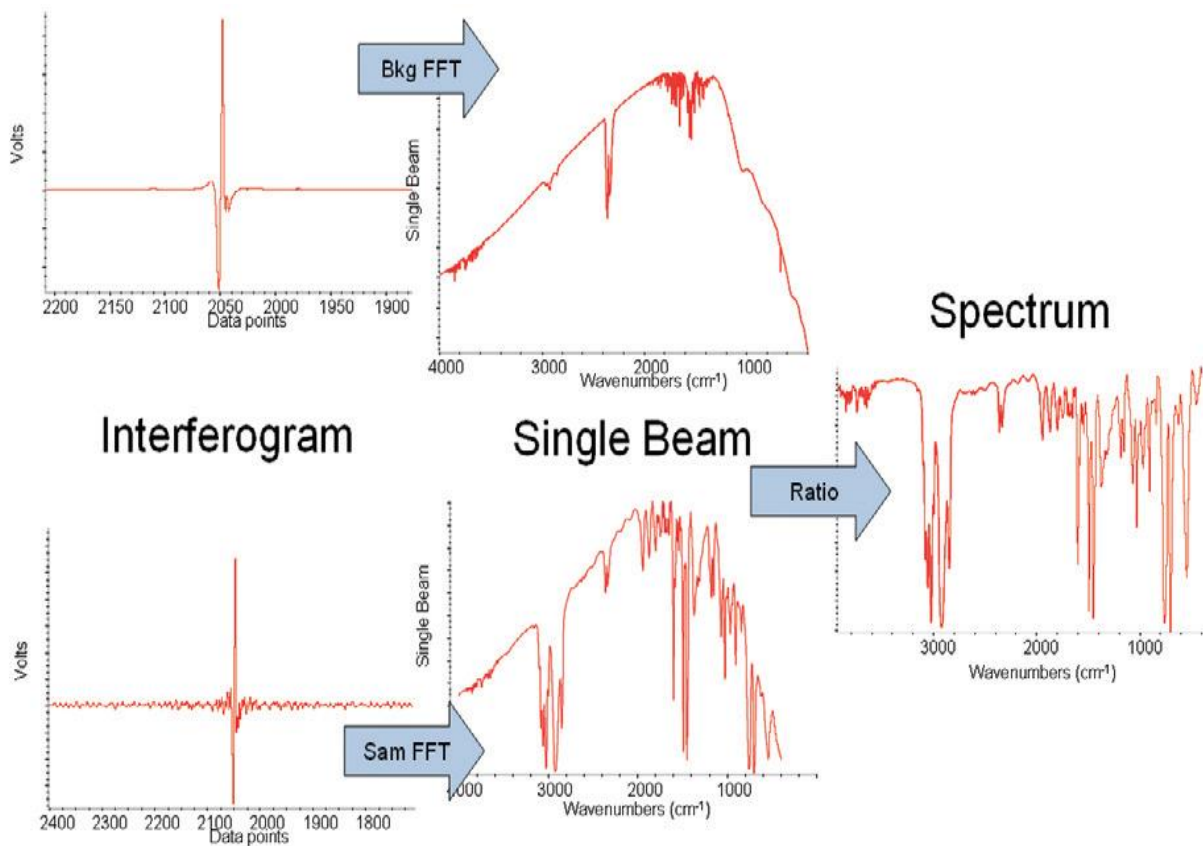
Fig.21: Schematic diagram of the process in obtaining an infrared spectrum **[source: ref. 40]**

The transmittance spectrum can be converted to absorbance by taking the negative $\log_{10}$ of the data points. Figure 21 shows a schematic diagram of the processes in obtaining an infrared spectrum.

The source of light used in a Fourier transform spectrometer is polychromatic. Each frequency give rise to a cosine shape signal and the resulting interferogram is the sum of all these. Mathematically, the detector signal and the interferogram are related to the spectrum by:

$$I(x) = \int_{-\infty}^{\infty} B(\upsilon) \cos(2\pi\upsilon x) d\upsilon \qquad (2.25)$$

Where I(x) is the intensity of the beam measured at the detector and x, the displacement of the movable mirror. B(υ) represents the intensity of the same as a function of the wavenumber (υ).

28

The spectrum is obtained through the inverse Fourier transform of the above relation and is given by:

$$B(\upsilon) = \int_{-\infty}^{\infty} I(x) \cos(2\pi\upsilon x) d\upsilon \qquad (2.26)$$

2.5.1 Advantages of Fourier Transform Spectrometer (FTS) over Grating Spectrometer

The Fourier Transform Spectrometer (FTS) does not separate the light into its frequency components before it is registered. Hence, each point in the interferogram consists of information about all wavelengths in the light source. Since all frequencies are measured simultaneously, most measurements are made in matter of seconds rather than several minutes. This is referred to as the Fellget advantage.

The Jacquinot advantage is another which implies that, more energy can be registered since the only light lost is the portion of the light that is reflected back to the light source. This leads to an increase in the signal- to- noise ratio.

Additionally, in a Fourier Transform Spectrometer, the resolution of the spectrum can be increased by increasing the scanning length of the moving mirror.

The Fourier Transform Spectrometer has an internal frequency standard, usually a HeNe laser. The moving mirror and the detector sampling interval are timed through the interference fringes that arise from the monochromatic light from this HeNe laser. All wavenumbers in the resulting spectrum are then calculated using the known laser frequency. This is called the Connes advantage.

The resolution in an FTS is the same for all wavenumbers while the resolution of the grating spectrometer is wavelength dependent.

One disadvantage of the FTS is, the light source has to be very stable since fluctuations in the light affect the inverse transform i.e. $B(\upsilon)$ is time dependent.

2.5.2 Interpretation of infrared spectra

The correlation of absorption bands in a spectrum of an unknown compound with known absorption frequencies for certain types of bonds are used in the interpretation of infrared spectra. Significant for the identification of the source of an absorption band are intensity (weak, medium or strong), shape (broad or shape) and position (cm^{-1}) in the spectrum. A brief summary of the infrared absorption frequencies of some functional groups is given in tables 1 and 2.

Functional Class	Stretching Vibrations			Bending Vibrations		
	Range (cm^{-1})	Intensity	Assignment	Range (cm^{-1})	Intensity	Assignment
Alkanes	2850-3000	str	CH_3, CH_2 & CH 2 or 3 bands	1350-1470 1370-1390 720-725	med med wk	CH_2 & CH_3 deformation CH_3 deformation CH_2 rocking
Alkenes	3020-3100 1630-1680 1900-2000	med var str	=C-H & $=CH_2$ (usually sharp) C=C (symmetry reduces intensity) C=C asymmetric stretch	880-995 780-850 675-730	str med med	=C-H & $=CH_2$ (out-of-plane bending) cis-RCH=CHR
Alkynes	3300 2100-2250	str var	C-H (usually sharp) C≡C (symmetry reduces intensity)	600-700	str	C-H deformation
Arenes	3030 1600 & 1500	var med-wk	C-H (may be several bands) C=C (in ring) (2 bands) (3 if conjugated)	690-900	str-med	C-H bending & ring puckering
Alcohols & Phenols	3580-3650 3200-3550 970-1250	var str str	O-H (free), usually sharp O-H (H-bonded), usually broad C-O	1330-1430 650-770	med var-wk	O-H bending (in-plane) O-H bend (out-of-plane)
Amines	3400-3500 (dil. soln.) 3300-3400 (dil. soln.) 1000-1250	wk wk med	N-H (1°-amines), 2 bands N-H (2°-amines) C-N	1550-1650 660-900	med-str var	NH_2 scissoring (1°-amines) NH_2 & N-H wagging (shifts on H-bonding)
Aldehydes & Ketones	2690-2840(2 bands) 1720-1740 1710-1720	med str str	C-H (aldehyde C-H) C=O (saturated aldehyde) C=O (saturated ketone)	1350-1360 1400-1450 1100	str str med	α-CH_3 bending α-CH_2 bending C-C-C bending

Table 1: Infrared absorption frequencies of functional groups. **[Source: ref. 41]**

30

IR Absorption Frequencies of Functional Groups Containing a Carbonyl (C=O)

Functional Group	Type of Vibration	Characteristic Absorptions (cm-1)	Intensity
Carbonyl			
C=O	stretch	1670-1820	strong
(conjugation moves absorptions to lower wave numbers)			
Acid			
C=O	stretch	1700-1725	strong
O-H	stretch	2500-3300	strong, very broad
C-O	stretch	1210-1320	strong
Aldehyde			
C=O	stretch	1740-1720	strong
=C-H	stretch	2820-2850 & 2720-2750	medium, two peaks
Amide			
C=O	stretch	1640-1690	strong
N-H	stretch	3100-3500	unsubstituted have two bands
N-H	bending	1550-1640	
Anhydride			
C=O	stretch	1800-1830 & 1740-1775	two bands
Ester			
C=O	stretch	1735-1750	strong
C-O	stretch	1000-1300	two bands or more
Ketone			
acyclic	stretch	1705-1725	strong
cyclic	stretch	3-membered - 1850 4-membered - 1780 5-membered - 1745 6-membered - 1715 7-membered - 1705	strong
α,β-unsaturated	stretch	1665-1685	strong
aryl ketone	stretch	1680-1700	strong

Table 2: Infrared absorption frequencies of carbonyl (C=O) functional groups. **[Source: ref. 42]**

2.5 Matrix isolation spectroscopy

Matrix isolation spectroscopy is a technique developed for the spectroscopic study of photochemically reactive, short-lived molecules trapped in a solid inert gas matrix. This technique helps to overcome some of the difficulties associated with the study of very reactive species. It is a successful approach for studying photochemical reactivity, taking advantage of the very low working temperature, which minimizes the available thermal energy and reduces the probability of occurrence of thermal reactions. The method involves trapping of the molecules in a rigid cage of a chemically inert substance (the matrix) at a very low temperature. The rigidity of the cage prevents diffusion of reactive molecules which would lead to reactions within this environment.
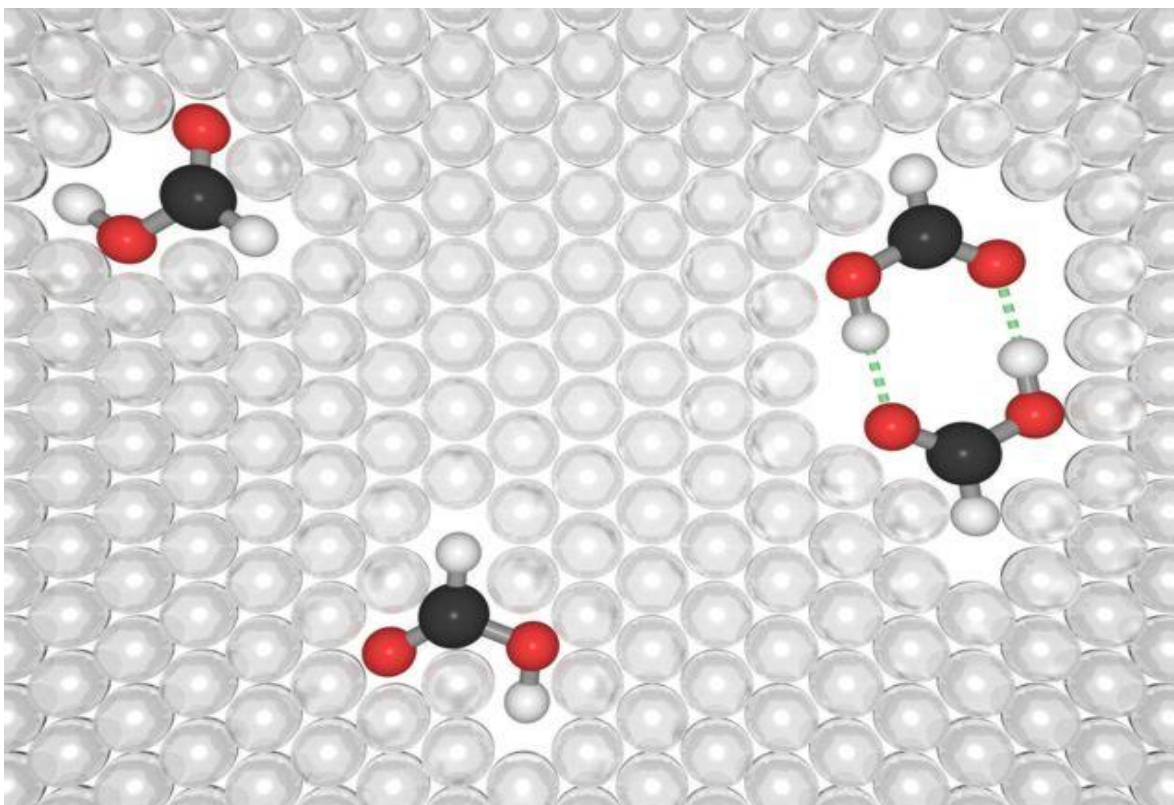
Fig.22: Sketch of formic acid (HCOOH) monomers and a formic acid dimer trapped in a matrix. **[Source: ref. 43]**

The low temperature contributes to the rigidity of the "matrix cage" and reduces the probability of internal rearrangements that require little activation energy. Few materials other than rare gases and nitrogen are chemically inert enough to serve as matrices for most reactive species. The formation of a rigid matrix requires the use of temperature not exceeding about one-third of the melting point of the solid e.g. temperatures of 29 K for argon, 26 K for nitrogen, etc. The most important factor, the low temperature, implies the use of cryogenic technology and in turn requires the use of high vacuum techniques without which low temperatures cannot conveniently be maintained. The nature of the matrix, the low temperature and the need to isolate the sample in a vacuum implies that only spectroscopic methods can be used to study matrix-isolated species in-situ and the experimental techniques is to a large extent dominated by the need to expose the sample to the beam of a spectrometer at the same time as cooling it in a high vacuum. [44] Figure 22 shows formic acid molecules (monomers and dimer) trapped in a rare gas matrix for illustration.

Chapter 3: Experimental work and results

3.1 Experimental setup

All the experimental work was carried out at the Alfred Wegener Institute (AWI) in Bremerhaven. The atmospheric chemistry laboratory there is equipped with instruments to perform experiments at cryogenic conditions and to study photochemical reactions by means of FTIR spectroscopy.
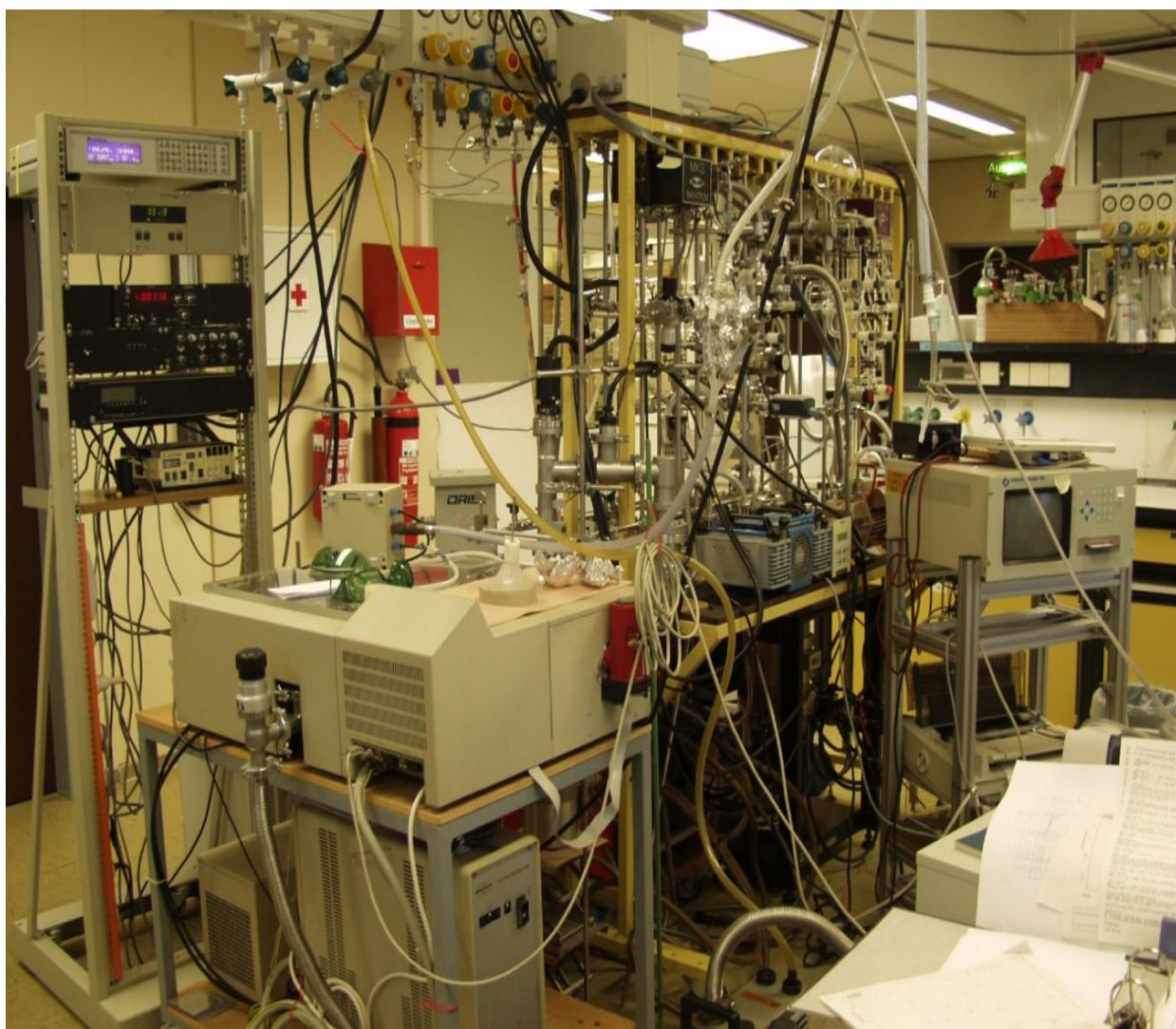
Fig.23: View of the complete experimental setup used with FTIR spectrometer, temperature controller, pressure control units, vacuum lines, etc.

The experimental setup includes a FTIR spectrometer, a vacuum pumping unit, gas handling lines and a cooling system consisting of a Helium compressor and a cryostat with a metal mirror on which the samples are deposited at low temperatures. The temperature can be controlled and varied by means of a temperature controller [see fig. 23]. The photolysis experiment can be carried out by means of a high-pressure mercury lamp. All the spectra were recorded in a reflection absorption infrared spectroscopy (RAIRS) mode. Details of the instruments in the laboratory used for these experiments are described in the subsequent sections below.

3.1.1 Fourier Transform Spectrometers

Infrared spectra were recorded on a Bruker IFS 66v FTIR spectrometer over a range of 600-4000 cm^{-1} of the different samples. The Bruker IFS 66v consists of a classical Michelson Interferometer with a maximum spectral resolution of 0.1cm^{-1}.
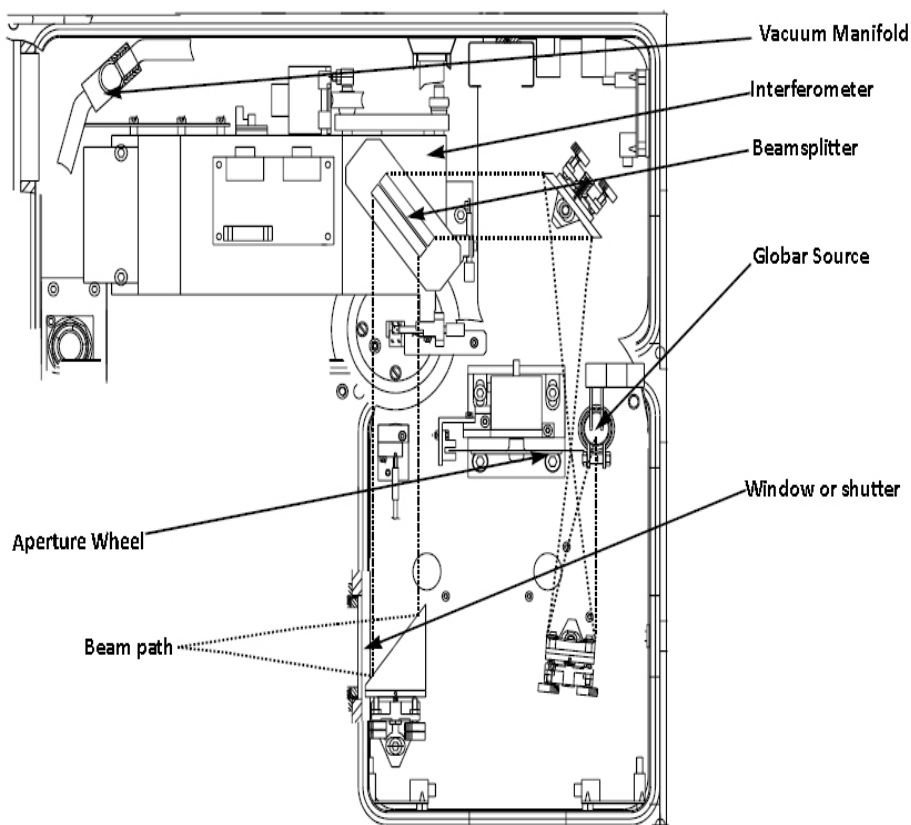
Fig. 24: Optical set-up (top-view) of the Bruker IFS 66v spectrometer **[source: ref. 45]**

It is equipped with a Globar as the infrared source, a liquid nitrogen-cooled MCT (Mercury Cadmium Telluride) detector and a germanium-coated KBr (Potassium bromide) beamsplitter. In the experiments reported here, measurements were taken at a resolution of $0.2 cm^{-1}$.

The gas phase spectra were measured with a Bruker IFS 55 Equinox FTIR spectrometer equipped with a Globar light source, nitrogen-cooled MCT detector and a germanium-coated KBr beamsplitter. Measurements were taken at a resolution of $0.5 cm^{-1}$.

3.1.2 Cryostat

Low temperature was required for the matrix isolation study, and in so doing, the system was maintained at a temperature of about 6K using a cryostat.

Fig.25: View of the cold head of the cryostat *(middle)* attached to the FTIR-spectrometer *(left)*

The cryostat used in this experiment is a combination of a LEYBOLD VACUUM COOLPAK 6000 compressor and a LEYBOLD VACUUM COOLPOWER 5/100 cold head. The temperature was measured by a LAKESHORE Model 340 temperature controller. Vacuum lines which were used for the gas handling and also as a deposition system had direct connection to the cryostat.

3.1.3 Photolysis System

The matrices and gas phase samples were photolysed with a 1000W Xenon-Mercury UV lamp (UXM 502MD) which is powered by an ORIEL 68820 universal power supply. Light from the lamp is passed through a 10 cm water filter interspaced between the lamp and the sample to reduce the infrared output of the lamp. A hose connects an ozone absorber to the UV lamp. In the experiments, 600W of electrical power was used for the photolysis. The spectral distribution of the relative intensity of the 1000W Xenon – Mercury UV lamp is shown in figure 27.
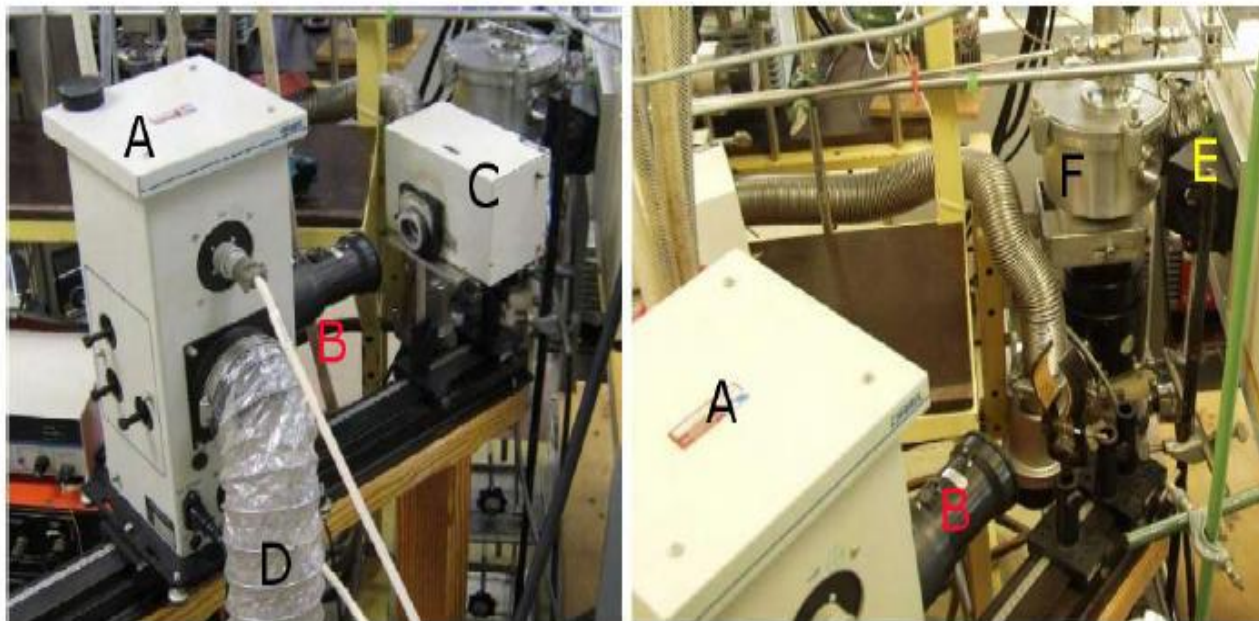
Fig.26: View of the Photolysis setup. **A.** UV lamp Cabinet **B.** Water Filter
C. Monochromator **D.** Hose connected to the ozone absorber, **E.** Spectrometer Unit, **F.** Cryostat Unit

USHIO UXM-502MD
spectral distribution
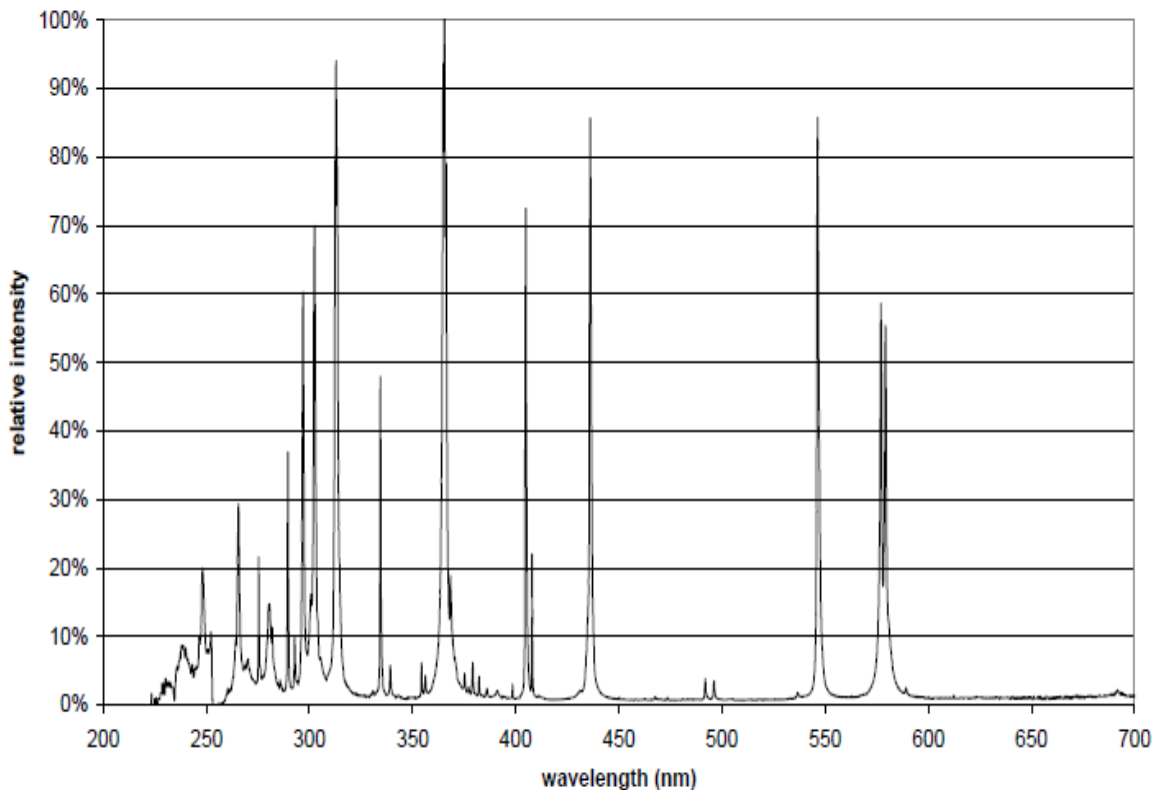
Fig.27 Spectral distribution of the relative intensity of the 1000W Xenon-Mercury
UV lamp.

3.2 Samples

3.2.1   Acetaldehyde (CH$_3$CHO)

Acetaldehyde is the second most abundant atmospheric aldehyde after formaldehyde and is considered to be an atmospheric pollutant, a component of photochemical smog and a potentially carcinogenic and mutagenic agent. **[46]** It plays an important role in the atmosphere as a source of ozone, peroxyacetyl nitrate and HOx radicals. It is classified as hazardous air pollutant by the US environmental Protection Agency (EPA, 1994). **[22]**

The concentration of acetaldehyde measured (or calculated) at ALERT 2000 at the end of April 2000, for example, was about 80 pptv over snow as compared to 40 pptv predicted by models that include only gas-phase chemistry (see table 3).

Species	Value measured over snow	Prediction by gas-phase chemistry (19)
HCHO	200 pptv	70 pptv
CH_3CHO	80 pptv	40 pptv
NO_x	25 pptv	1 pptv
HONO	20 pptv	1 pptv
OH	0.03 pptv*	0.003 pptv
HO_2	3.7 ppt*	0.9 ppt
O_3	As low as 0.07 ppb	30–34 ppbv
Hg^0	0.02 pptv	0.17 pptv

*Calculated in (19, 20).

Table 3: Measured concentrations of gaseous species at ALERT 2000. **[Source ref: 11]**

D. Grosjean et al. [47] measured ambient levels of acetaldehyde in three major urban areas of Brazil: Sao Paulo, Rio de Janeiro and Salvador was up to 63 ug/m^3 or 35ppb.

The chemical formula of acetaldehyde is CH_3CHO and a molecular structure as shown in figure 28.
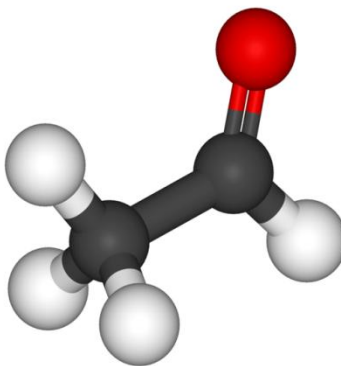
Fig.28: Molecular structure of acetaldehyde **[Source: ref. 48]**

Acetaldehyde is released into the atmosphere by anthropogenic and natural sources. Sources of atmospheric acetaldehyde include the photochemical degradation of volatile organic compounds (VOCs) such as >C$_1$ alkanes and >C$_2$ alkenes which is thought to be the largest source. Also the

oxidation of isoprene (C_5H_8) and ethanol (C_2H_5OH) are known to tribute to the global acetaldehyde budget for which ethanol is of particular interest since it is used as an alternative fuel (ethanol fuel) for cars in most south American countries **[17,22].**
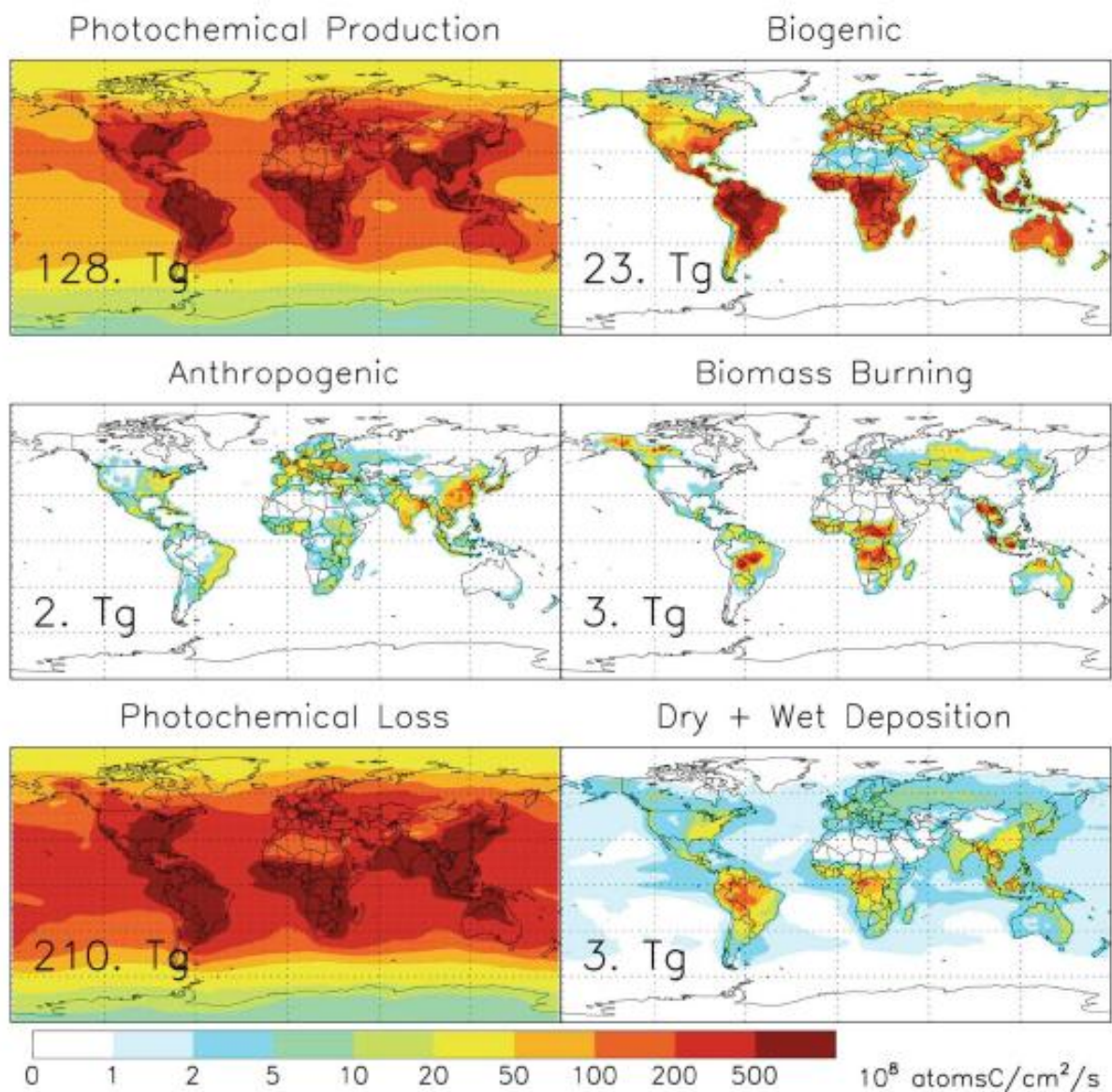
Fig 29. Annual average sources and sinks (2004) of acetaldehyde in GEOS-chem. Shown are photochemical production, biogenic emissions from live and decaying plants, anthropogenic emissions (urban/industrial + biofuel), biomass burning emissions, photochemical loss (OH + photolysis), and deposition.**[source: ref. 22]**

Acetaldehyde is emitted directly into the atmosphere also by terrestrial plants as a result of fermentation reactions leading to ethanol production in leaves and roots. Urban and industrial activities mainly as by-products of combustion and from its production and use as chemical intermediates are sources of atmospheric acetaldehyde. Other sources of atmospheric acetaldehyde include biomass burning, biofuel burning and it is also produced in surface waters by photodegradation of coloured dissolved organic matter (CDOM) which are subsequently 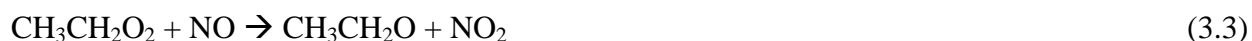emitted into the atmosphere **[22,49]. D.B. Millet et al. 2010, [22]** used a 3-D chemical transport model (GEOS-chem. CTM) to develop a detailed global budget for sources and sinks of atmospheric acetaldehyde for 2004. Results obtained with this model are shown in figure 29.

Among the natural sources of acetaldehyde in the atmosphere is the tropospheric oxidation of nonmethane hydrocarbons (NMHC), e.g. various alkanes and olefins bearing one methyl substituent such as propene. **[49]**

The formation of acetaldehyde in the troposphere from the oxidation of ethane is described by the reaction below:

$$CH_3CH_3 + OH \rightarrow CH_3CH_2 + H_2O \qquad\qquad (3.1)$$

$$CH_3CH_2 + O_2 \rightarrow CH_3CH_2O_2 \qquad\qquad (3.2)$$

$$CH_3CH_2O_2 + NO \rightarrow CH_3CH_2O + NO_2 \qquad\qquad (3.3)$$

$$CH_3CH_2O + O_2 \rightarrow \textbf{CH}_3\textbf{CHO} + HO_2 \qquad\qquad (3.4)$$

The removal of acetaldehyde from the atmosphere occurs mostly by chemical or photolytic degradation and also by dry or wet deposition. This is further illustrated in figure 29. This renders the lifetime of acetaldehyde in the order of several days. Of these processes, the most important one is the oxidation initiated by the reaction with hydroxyl radical (OH) described by the reactions below, rendering the lifetime on the order of one day. **[22]**

$$CH_3CHO + OH \rightarrow CH_3CO + H_2O \qquad\qquad (3.5)$$

$$CH_3CO + O_2 \rightarrow CH_3(CO)O_2 \qquad\qquad (3.6)$$

$$CH_3(CO)O_2 + NO \rightarrow CH_3 + CO_2 + NO_2 \qquad\qquad (3.7)$$

$$CH_3 + O_2 \rightarrow CH_3O_2 \qquad\qquad (3.8)$$

$$CH_3O_2 + NO \rightarrow CH_3O + NO_2 \qquad\qquad (3.9)$$

$$CH_3O + O_2 \rightarrow HCHO + HO_2 \qquad\qquad (3.10)$$

$$HO_2 + NO \rightarrow NO_2 + OH \qquad\qquad (3.11)$$
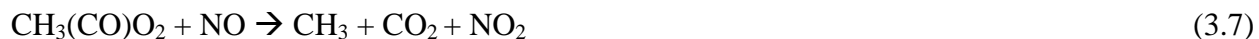
The oxidation of acetaldehyde may lead to the formation of peroxyacetylnitrate ($CH_3(CO)O_2NO_2$) which is a component of the photochemical smog. This is described by the reaction below;

$$CH_3CHO + OH \rightarrow CH_3CO + H_2O \qquad\qquad (3.12)$$

$$CH_3CO + O_2 + M \rightarrow CH_3(CO)O_2 \qquad\qquad (3.13)$$

$$CH_3(CO)O_2 + NO_2 + M \rightarrow \textbf{CH}_3\textbf{ (CO)O}_2\textbf{NO}_2 \qquad\qquad (3.14)$$
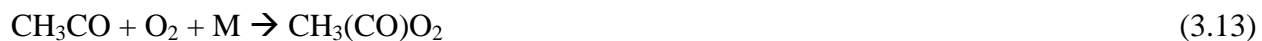
Many authors have reported studies of the photodissociation of acetaldehyde in the gas phase whereby three pathways have been suggested:

$$CH_3CHO + h\nu \rightarrow CH_3 + CHO \quad (\lambda \leq 330 \text{ nm}) \qquad 1 \qquad (3.15)$$

$$\rightarrow CH_4 + CO \quad (\lambda \leq 292 \text{ nm}) \qquad 2 \qquad (3.16)$$

$$\rightarrow CH_3CO + H \quad (\lambda < 320 \text{ nm}) \qquad 3 \qquad (3.17)$$
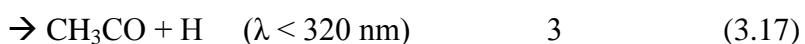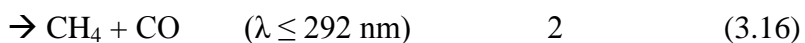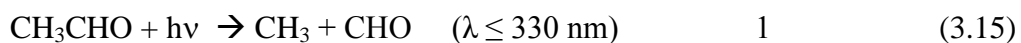
The first channel is of importance at tropospheric conditions and has been observed as the major channel upon photoexcitation of CH_3CHO at 318 nm. Channel 2 has been reported to have a high quantum yield of 0.6-0.7 at 254nm whereas channel 3 has very small quantum yields (0.025 at 300 nm, decreasing to zero at 320 nm) and does not contribute significantly. The radicals products from channels 1 and 3 may also undergo subsequent dissociation and reactions to form CH_3 + CO +H. As a result of all these experiments, it has been concluded that channel 1 originates from a vibrationally excited triplet state of acetaldehyde while channel 2 and 3 become increasingly important at shorter wavelengths and occur from the high vibrational levels of the first excited singlet state. **[50, 51, 52, 53, 54]**
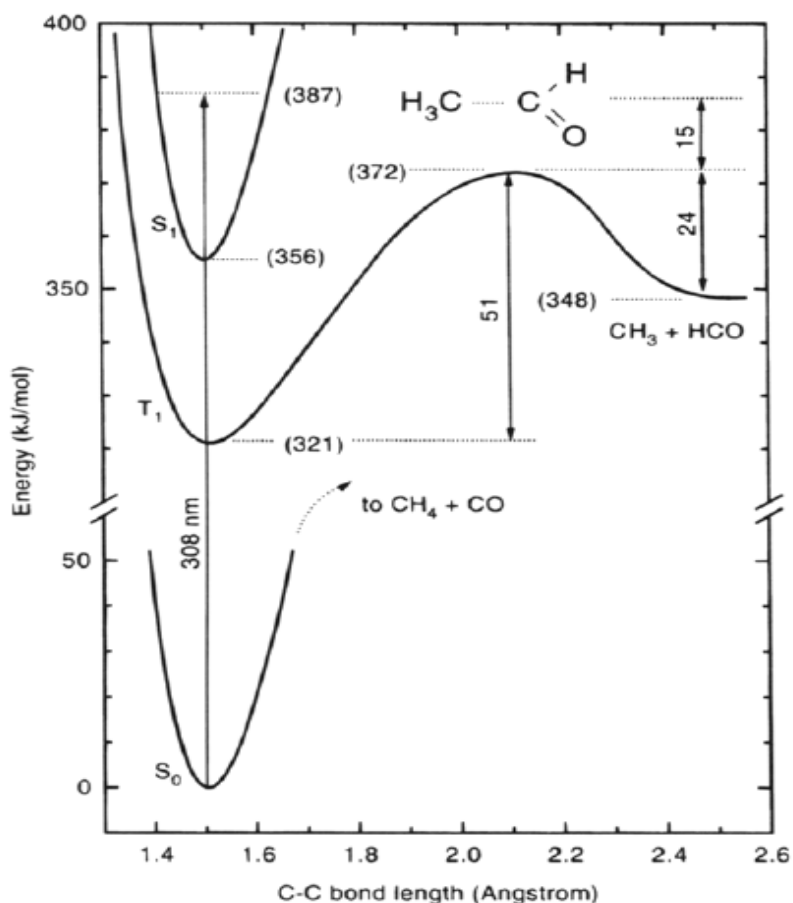
Fig. 30: Schematic potential energy diagram for the electronic states of acetaldehyde
[source: ref 53]

43

In figure 30, a schematic potential energy diagram of the electronic states of acetaldehyde relevant to photodissociation in the range of 250nm – 350nm is shown which corresponds to transition to the S_1 state (excited singlet state).

At wavelengths shorter than 320 nm, CH_3CHO dissociates to CH_3 + CHO. This dissociation mechanism involves an intersystem crossing from the S_1 potential energy surface to the lower triplet surface T_1 on which the dissociation proceeds over a small barrier. **[50, 51, 52, 53, 54]**

The UV absorption cross section of acetaldehyde at a temperature of 294K and a resolution of 0.08nm is shown in figure 31. Absorption increases gradually from 200nm to about 300nm then it decreases right after 300nm. Maximum absorption for acetaldehyde occurs between 280nm – 300nm.
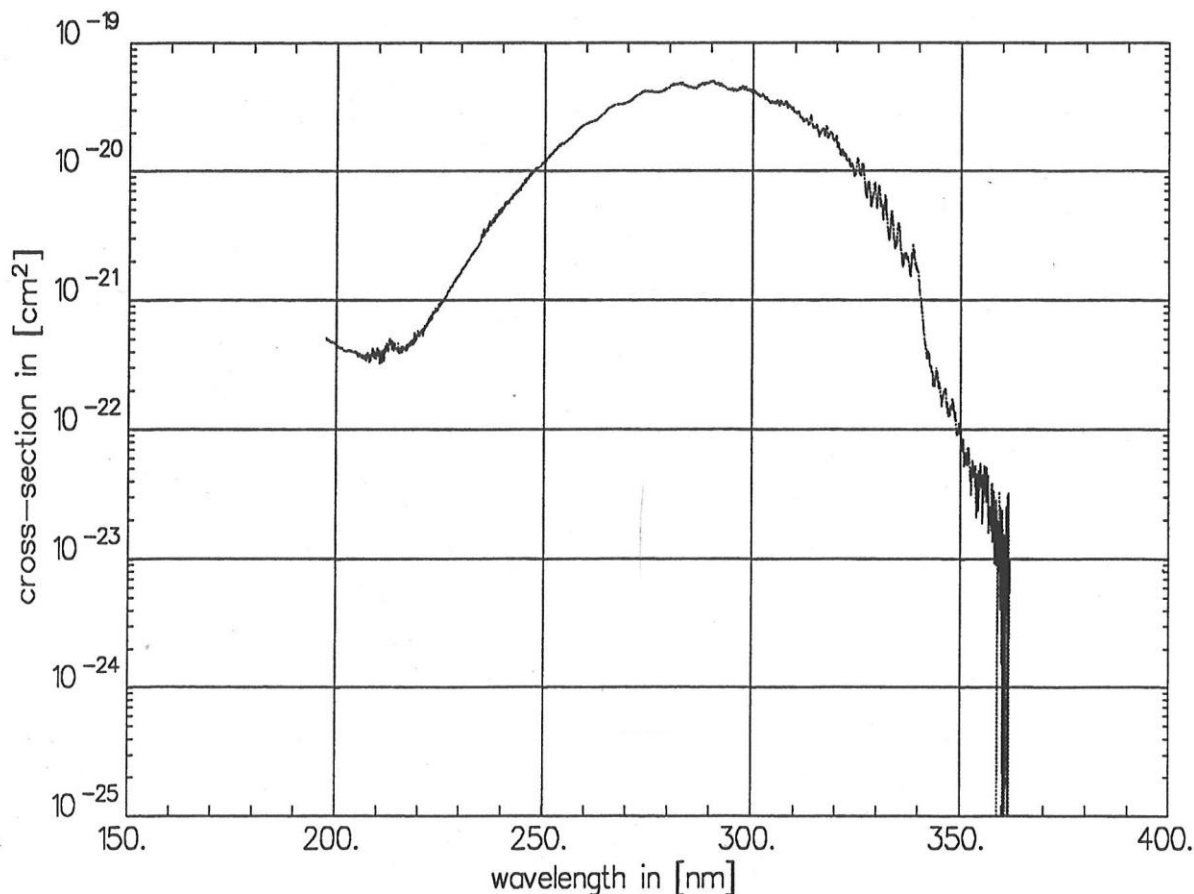
Fig. 31. UV absorption cross section of acetaldehyde **[Source: ref. 55].**

3.2.2 Acrylic acid (CH$_2$CHCOOH)

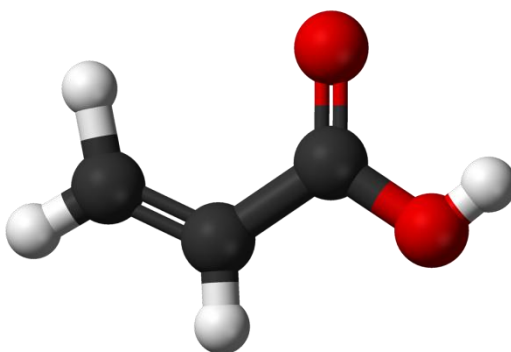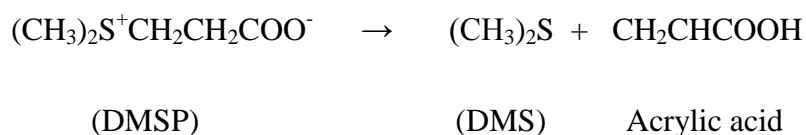Acrylic acid is one of the moderately strong carboxylic acids that exist in the atmosphere. Its odour has been described as irritating, acrid and pungent. Its chemical formula is CH$_2$CHCOOH and a molecular structure as shown in figure 32:

Fig. 32 Molecular structure of acrylic acids **[Source: ref. 56]**

Acrylic acid has both natural and anthropogenic sources. The most important natural source is from certain species of algae in seawater and ice. These algae produce dimethylsulphoniopropionate (DMSP) which decomposes into dimethyl sulphide (DMS) and acrylic acid which are subsequently released into the atmosphere **[20]**. This is illustrated by the equation below:

$$(CH_3)_2S^+CH_2CH_2COO^- \quad \rightarrow \quad (CH_3)_2S \; + \; CH_2CHCOOH$$

$$\text{(DMSP)} \qquad\qquad\qquad \text{(DMS)} \qquad \text{Acrylic acid}$$

Acrylic acid has also been found to occur naturally in certain species of marine algae such as phaeocystis and polysiphonia lanosa. It has been found in oysters, scallops, digestive tract of penguins and rumen fluid of sheep. Anthropogenic sources of acrylic acid are mainly from the chemical products sector and plastic products industries. These include industries producing industrial organic chemicals, plastics, resins, soaps, cleaning compounds, adhesives and other chemical and plastic products. All these industries emit significant amounts of acrylic acid into the atmosphere. In the atmosphere, acrylic acid undergoes chemical and photochemical

reactions. Chemical reactions include rapid polymerization in the presence of oxygen. Acrylic acid is removed from the atmosphere by reacting photochemically with hydroxyl radicals and ozone which produces glyoxylic acid and formic acids as intermediates and hydrogen peroxide and citric acid as end products. Other sinks of acrylic acid include dry and wet deposition. Acrylic acid is biodegradable. It is also destroyed by sunlight in surface soils and water. It is slightly persistent in water but will degrade. All these processes renders the atmospheric lifetime of acrylic acid to be few days to weeks. [57] Many scientists have reported about the gas phase photodisssociation of acrylic acid whereby several processes have been proposed as primary dissociation channels. [26, 27, 28]

$$CH_2CHCOOH + h\nu \rightarrow CH_2CH + HOCO \qquad\qquad 1 \qquad\qquad (3.18)$$

$$\rightarrow CH_2CHCO + OH \qquad\qquad 2 \qquad\qquad (3.19)$$

$$\rightarrow CH_2CH_2 + CO_2 \qquad\qquad 3 \qquad\qquad (3.20)$$

$$\rightarrow CH_2COH + CO \qquad\qquad 4 \qquad\qquad (3.21)$$

It has been reported that channels 1 and 2 yield radical products from C-C and C-O bond cleavage respectively while channels 3 and 4 represents decarboxylation and decarbonylation reactions respectively. [27, 58]
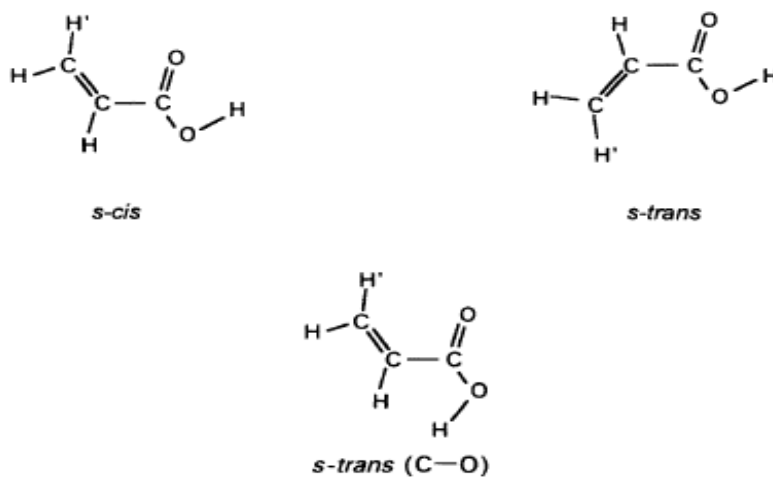
Fig.33 Conformers of acrylic acid monomer **[source: ref. 25]**

Acrylic acid can exist in different conformers. Most often the presence of these conformational isomers can be observed in the IR spectrum of acrylic acid (see fig. 33).

3.3 Experimental work

Acetaldehyde used in this experiment was purchased from Sigma-Aldrich Chemie GmbH (Fluka Analytical) with a vapour pressure of 756.4 mm Hg at 20˚C, boiling point at 21˚C and melting point at -125˚C. The acetaldehyde was 99.5% pure but was further purified by repeated freeze, pump and thaw cycles while the gas line were evacuated using the vacuum lines.

Gas phase spectra of acetaldehyde (p = 10mbar in a 10 cm gas cell) was recorded using the Bruker IFS 55 Equinox spectrometer. After recording the spectrum the sample was irradiated in time intervals of 30 seconds. In all cases, the growth rates of the photoproducts were noted and a graph of the growth of these photoproducts was plotted.

For the experiments in the solid phase, the cold head of the cryostat with the sample holder (Al mirror) was cooled to a very low temperature. This was necessary in order to make measurements of the sample trapped in different matrices (solid rare gases, O_2, H_2O ice and D_2O ice). Mixtures were mixed in the vacuum manifold at different mixing ratios in a 1-litre glass bulb at room temperature and deposited onto the Al mirror in the cold head of the cryostat. The vacuum manifold was routinely evacuated before each mixture was prepared. Background spectra were recorded using the IFS 66v spectrometer after which the mixture was deposited on the mirror and spectra recorded. The mixture was then irradiated using the UV lamp at different time intervals after which spectra of photolysed samples were recorded. All spectra were recorded in the reflection mode as stated earlier (see fig. 34).

A similar procedure was followed in preparation and in taking measurements of acrylic acid trapped in solid argon and H_2O ice. The acrylic acid was purchased from Sigma-Aldrich Chemie GmbH which was 99% pure. It has melting point of 14^oC, boiling point of 141^oC and a vapour pressure of about 3mmHg at 20^oC.
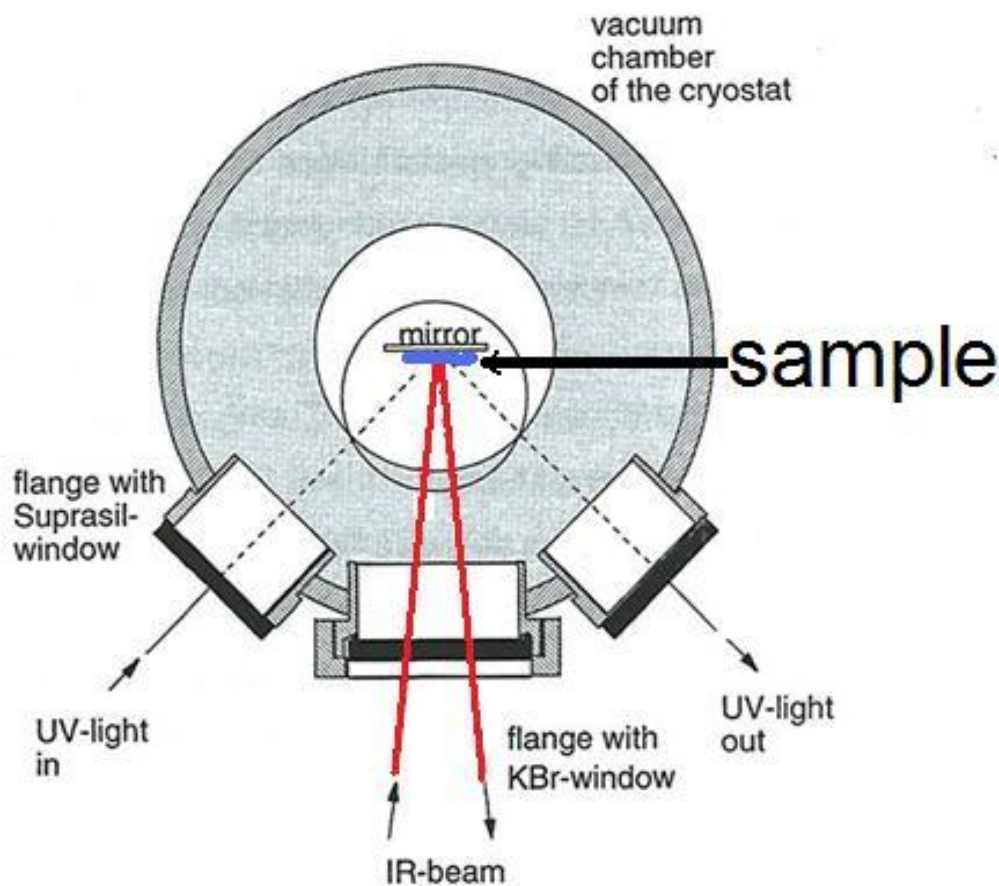
Fig. 34 Schematic view of the cold head of the cryostat

3.4 Results and Discussions

3.4.1 Acetaldehyde (CH$_3$CHO)

The gas phase (10 mbar CH$_3$CHO in a 10 cm gas cell) and rare gas matrices spectra are shown in figures 35 and 37, respectively. The absorption bands observed were assigned to the fundamental vibrations of acetaldehyde and summarized in table 4. The assignments were based on the works by **C.O. Della Vedova et al. [17], T. Shimanouchi [59] and   H. Zhao et al. [60].**

The IR spectra of gaseous acetaldehyde was recorded before and after irradiation at time intervals in shown in figure 35.
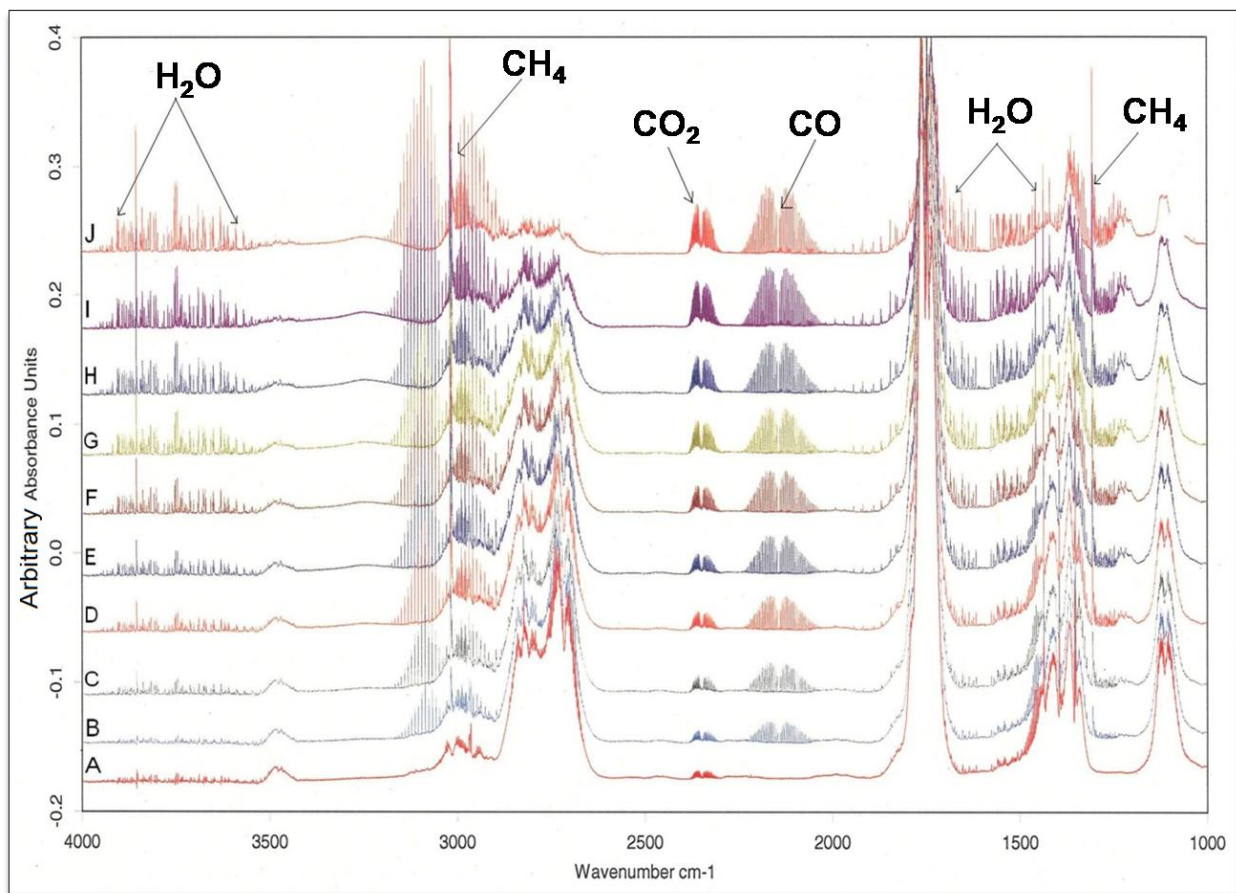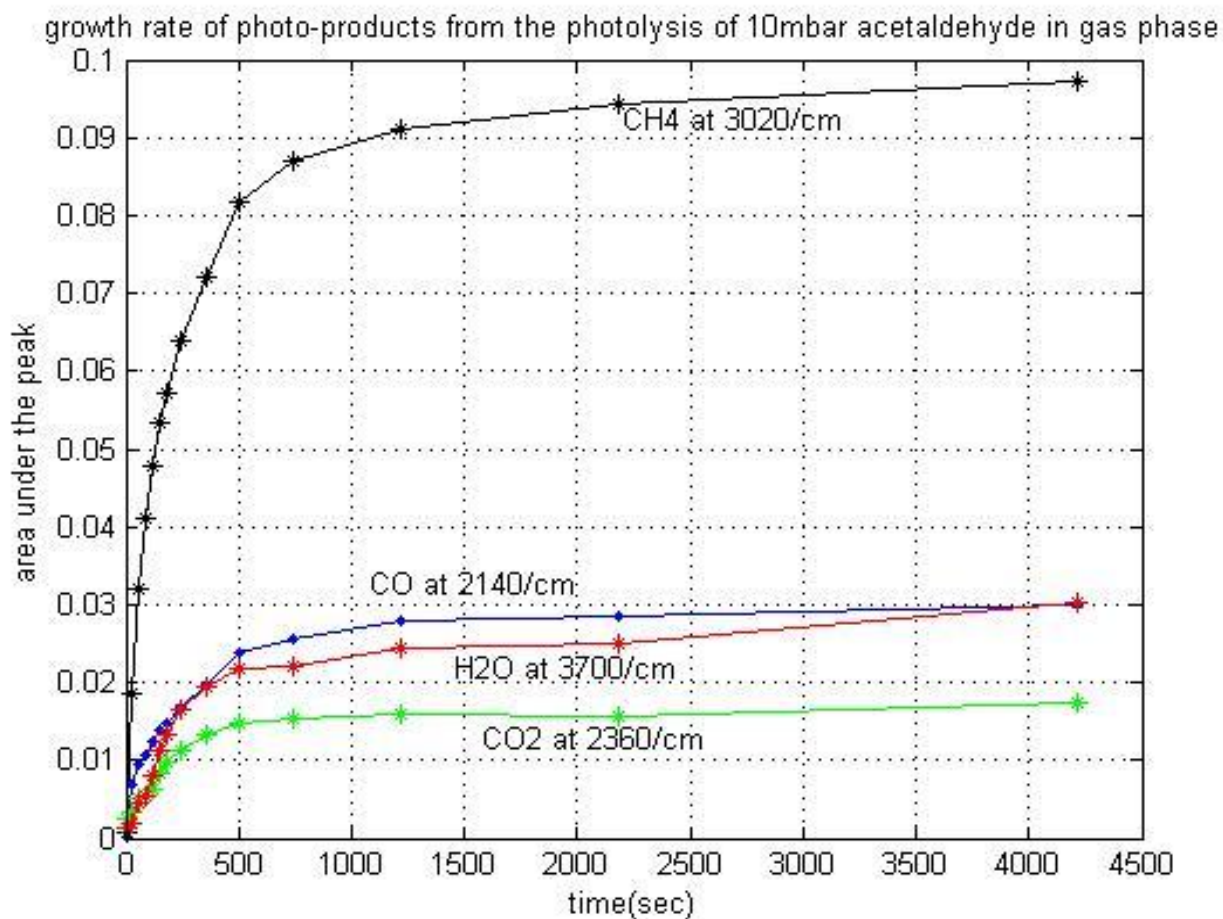
Fig.35: IR spectrum of acetaldehyde in the gas phase (10 mbar in 10 cm gas cell) Before (**A**) and after **B.** 30sec **C.** 60sec **D.** 90sec **E.** 120sec **F.** 150sec **G.** 180sec **H.** 240sec **I.** 360sec **J.** 500sec irradiation with a 1000W Xenon-Mercury UV lamp.

After photolysis of the 10 mbar gas phase acetaldehyde, most of the infrared absorptions corresponding to acetaldehyde disappeared and new bands appeared mostly in the regions of around 3000 cm^{-1}, 2130 cm^{-1}, 2350 cm^{-1}, and 1300 cm^{-1}. The absorption in the region of around 2130cm^{-1} is caused by the CO stretching vibration of the CO molecule, whereas both bands around the regions of 3000 cm^{-1} and 1300 cm^{-1} were caused by the CH_4 molecule, that is, the asymmetric C-H stretching and C-H deformation modes, respectively. Absorption bands of CO_2 appeared at 2350 cm^{-1} and of H_2O at 3200 – 4000 cm^{-1} and around 1600 cm^{-1}.

A graph of the growth rate of the photoproducts after photolysis from 30 sec to 4220sec is displayed in figure 36. From the graph, the photoproducts of acetaldehyde (CO and CH_4) had strong increases until about 1200 sec photolysis time. Thereafter it appeared to increase only

49

slowly. This was attributed to the higher acetaldehyde concentration in the first 20 min of the reaction leading to the increase in photoproducts until about 1200sec. When most of the acetaldehyde molecules were photolysed the growth rate decreases. The appearance of H_2O and CO_2 in the spectra may be attributed at least to some extent to ambient air. In addition, further reactions of the radicals produced in channels 1 and 3 during the photodissociation of acetaldehyde as discussed in section 3.2.1 may result in the production of secondary products and in this case H_2O and CO_2.

Fig.36: Growth curve of photoproducts of acetaldehyde photolysis in the gas phase

The IR difference spectra of acetaldehyde trapped in solid rare gases matrices at a temperature of 6 K and a mixing ratio of 1/1000 is shown figure 37. Absorption bands pointing downwards are

diminishing acetaldehyde bands as well as new photoproducts after several minutes of irradiation are pointing upwards.
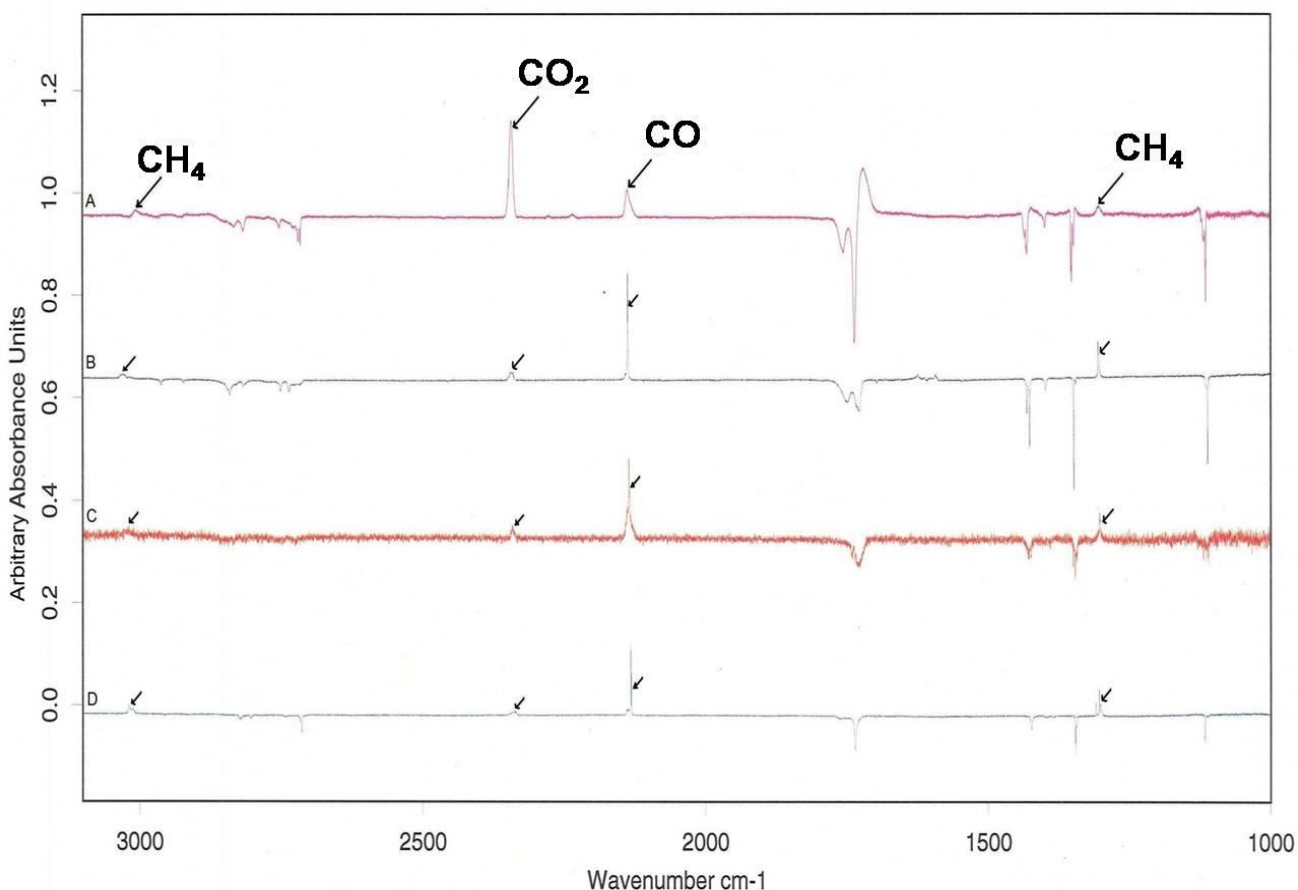
Fig.37 IR difference spectra of CH_3CHO trapped in solid rare gases at $T = 6K$ (ratio: 1/1000)   **A.** CH_3CHO /Ne after 30min irradiation   **B.** CH_3CHO / Ar after 305min irradiation   **C.** CH_3CHO / Kr after 135min irradiation   **D.** CH_3CHO / Xe after 75min irradiation .

The photoproducts of acetaldehyde which were observed in the rare gas matrices were CO and CH_4 and the formation of these products can be interpreted by the reaction below:

$$CH_3CHO + h\nu \longrightarrow CH_3 + CHO \xrightarrow{\text{(matrix)}} CH_4 + CO \qquad (3.15)$$

It was observed that the absorption frequencies of the photoproducts in the various matrices are different (i.e. there was a shift in the wavenumbers of the photoproducts). This is caused by the different strengths of the van-der Waals type interaction between the CH_3CHO guest molecules in the different rare gas matrix cages. The more electrons the rare gas has, the stronger the

interaction with the observed molecule. This can be seen from the data summarized in table 5. The formation of CO_2 is attributed to the formation of acetaldehyde dimers in the matrices. The higher amount of CO_2 as observed in neon matrix was due to about ≤ 0.5ppmv of CO_2 in the neon gas used in this experiment. In addition neon matrices are very soft at 6K allowing diffusion of the trapped guest molecules. In our case it means the formation of CH_3CHO dimers is more likely than in the other rare gas matrices and thus additional photoproducts (e.g. CO_2) can be expected.

Gas phase (cm^{-1})	Ne (cm^{-1})	Ar (cm^{-1})	Kr (cm^{-1})	Xe (cm^{-1})	H_2O-ice (cm^{-1})	O_2 (cm^{-1})	Assignments
3014	3013	3011	3009	3006	3022	3014	ν_{as} CH_3
2964	2968	2962	2960	2956	2933	2971	ν_s CH_3
2823	2852	2840	2832	2821	2839	2839	CH stretch
2752	2753	2750	2745	2743	2794	2739	CH stretch
2729	2719	2736	2724	2713	-	-	ν CH
1761	1756	1749	1740	1735	1737/1686	1755/1697	ν CO
1436	1431	1431	1429	1423	1415	1432	δ CH
1394	1399	1398	1404	1398	1375	1399	δ_{as} CH_3
1352	1357	1348	1346	1345	1303	1350	δ_s CH_3
1111	1119	1111	1113	1116	1115	1111	ν CC

Table 4: Fundamental vibrations of acetaldehyde in gas phase and the various matrices

PRODUCTS	Ne (cm^{-1})	Ar (cm^{-1})	Kr (cm^{-1})	Xe (cm^{-1})
CO	2142	2135	2132	2128
CH$_4$	1313	1306	1302	1299
CO$_2$	2352	2344	2341	2337

Table 5: Product bands from the photolysis of the various rare gas matrices

IR spectra of acetaldehyde trapped in solid O_2 before and after irradiation were recorded. Photoproducts such CO, CO_2 and CH_4 were observed as well as other photoproducts that are assigned in a similar work by **J.R. Sodeau et al. 1990. [ref. 50]**
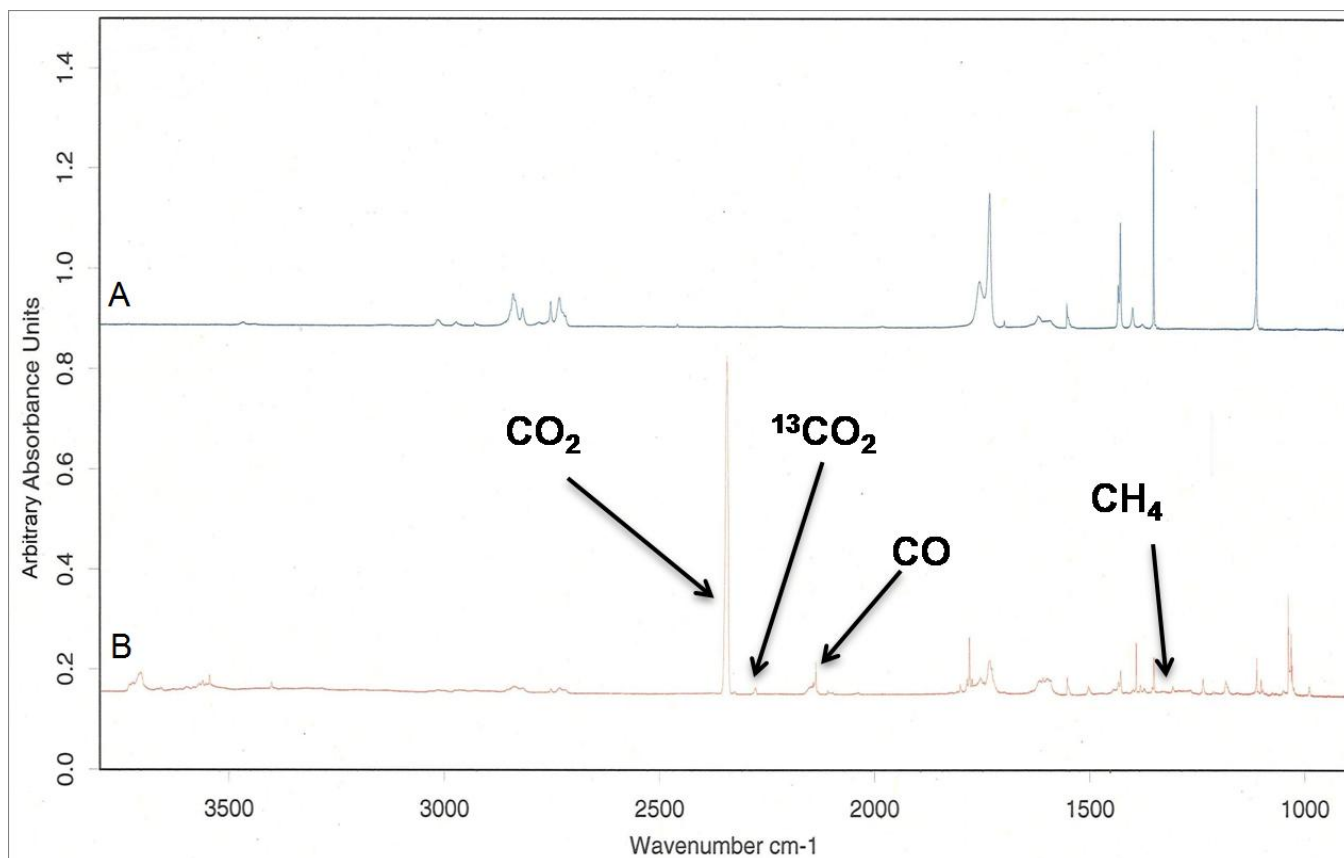
Fig.38: IR spectra of a matrix $CH_3CHO:O_2 = 1:1000$ at 6K before (A) and (B) after 10min photolysis

The first IR spectra, before and after irradiation of CH_3CHO trapped in H_2O ice was recorded at a temperature of 20 K in a mixing ratio (1:6). Photoproducts observed were mainly CO_2, CO, and CH_4 (see fig. 39).

IR spectra of $CH_3CHO:D_2O$, $CD_3CDO:Ar$, $CD_3CDO:H_2O:Ar$, $CD_3CDO:D_2O$ after deposition were recorded with the absorption bands assigned to their fundamental vibrations in each case (see table 6). The assignments were made in comparison to works done by **T. Shimanouchi [59]**. Absorption bands involving the deuterium in each case shifted to a lower wavenumber as compared to those involving hydrogen in $CH_3CHO:H_2O$ ice and other solid rare gases. This is attributed to the mass difference of Deuterium as compared to Hydrogen.
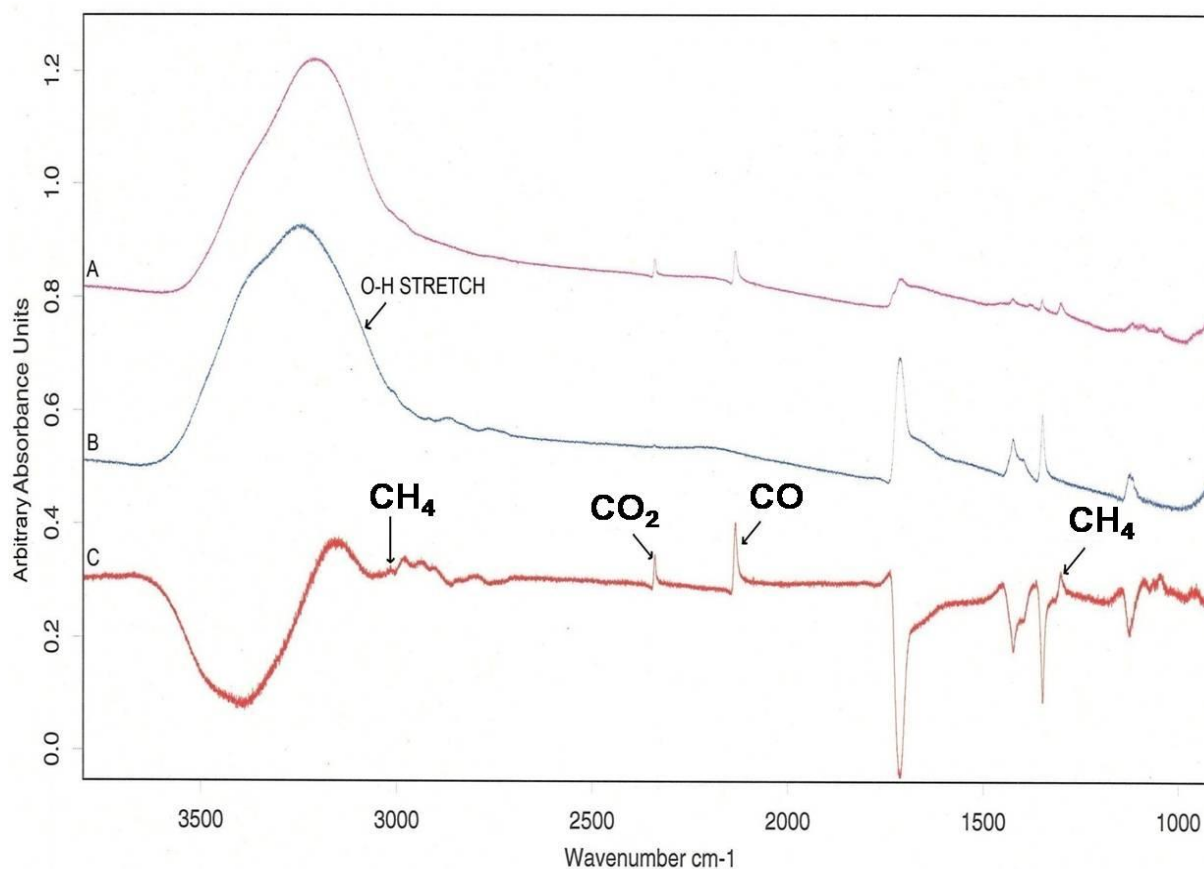
**Fig.39** IR Spectra of CH_3CHO trapped in H_2O ice at T= 20 K (ratio: 1/6)

A. After 490min   irradiation **B.** After deposition **C.** difference spectrum

The IR difference spectra (before and after photolysis) of $CH_3CHO:Ar$ (1:1000) at temperature 6K irradiated with the UV lamp at 600W for 300min and $CD_3CDO:Ar$ (1:1000) at 6K

photolysed for about 675min are shown in figure 40. New absorption bands which appeared after UV irradiation points upwards while diminishing acetaldehyde absorption bands points downwards. Asymmetric C-H stretching vibration and C-H deformation modes of CH_4 were observed in CH_3CHO:Ar at 3000cm^{-1} and 1300cm^{-1} respectively whereas the asymmetric C-D stretching vibration and C-D deformation modes of CD_4 (deuterated methane) observed in CD_3CDO:Ar at around 2250cm^{-1} and 995cm^{-1}, respectively. The absorption band in the region of 2350cm^{-1} in both spectra is due to the asymmetric C-O stretching vibration of the CO_2 molecule. The appearance of the CO_2 molecule is a result of the formation of acetaldehyde dimers in both matrices. The C-O stretching vibration of the CO molecule appeared at 2137cm^{-1} in both cases but in CD_3CDO:Ar another CO band appeared at 2115cm^{-1} which may be due to different spatial orientation of the molecule in the matrix. Changes in the intensities of the CO molecule's absorption band are due to isolated molecules in the matrix.

CD$_3$CDO:Ar (cm^{-1})	CD$_3$CDO:H$_2$O (cm^{-1})	CD$_3$CDO:H$_2$O:Ar (cm^{-1})	CD$_3$CDO:D$_2$O (cm^{-1})	Assignments
-	3200-3550	3250 – 3500	3220 -3500	O-H stretch
-	-	-	2400-2600	D-O stretch
2266	2153	2127	2145	υ_{as} (CD$_3$)
2126	2125	2098	2108	υ_s (CD$_3$)
2098	2112	2062	2110	υ (C-D)
1726	1712	1741	1711	υ (C-O)
1691	1694	1684	1693	υ (C-O)
1151	1166	1147	1166	υ (C-C)
1044	1042	1044	1031	δ_{as} (CD$_3$)
1023	1023	1023	1017	δ_s (CD$_3$)
949	950	949	960	δ (C-D)

Table 6: Fundamental vibrations of deuterated acetaldehyde various matrices
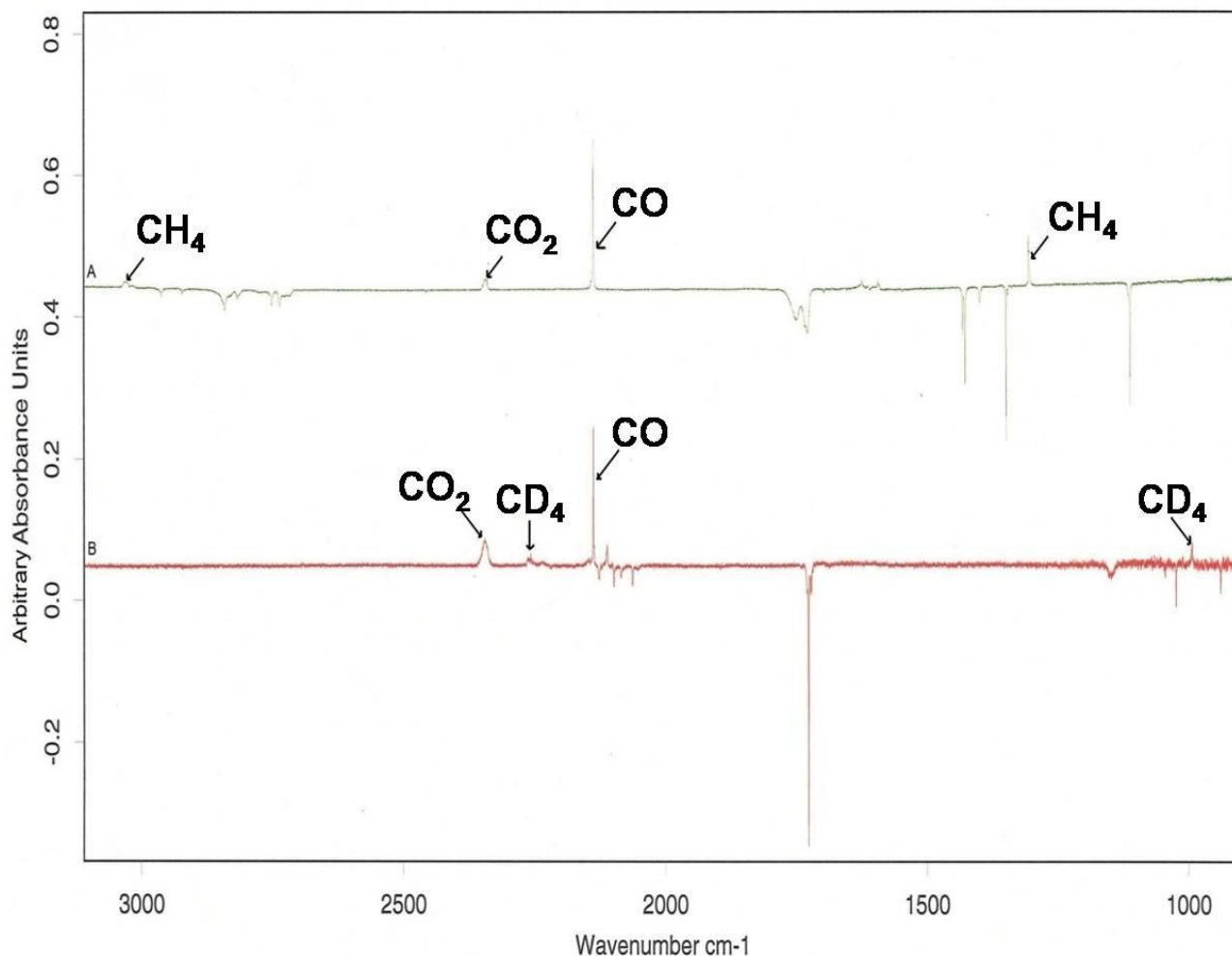
Fig.40 IR difference spectra of CH_3CHO/Ar and CD_3CDO/Ar at T=6K
A. CH_3CHO/Ar after 300min irradiation **B.** CD_3CDO/Ar after 675min irradiation

IR spectra of $CH_3CHO:D_2O$ (1:11) at a temperature of 14 K before and after UV irradiation for about 630min is illustrated in figure 41. The broad absorption band around 3310cm^{-1} is attributed to O-H stretching vibration of H_2O ice which might have resulted from traces of water vapour on the walls of the gas handling lines. O-D stretching vibration of D_2O ice was observed at around 2535cm^{-1}. Asymmetric C-H stretching vibration and C-H deformation modes of CH_4 were observed around 3008cm^{-1} and 1303cm^{-1} respectively. Photoproducts of CO_2 and CO absorption band appeared around 2342cm^{-1} and 2133cm^{-1} respectively. Small absorption band around 2235cm^{-1} is attributed to N_2O molecule from ambient air or maybe a leak in the system**.**
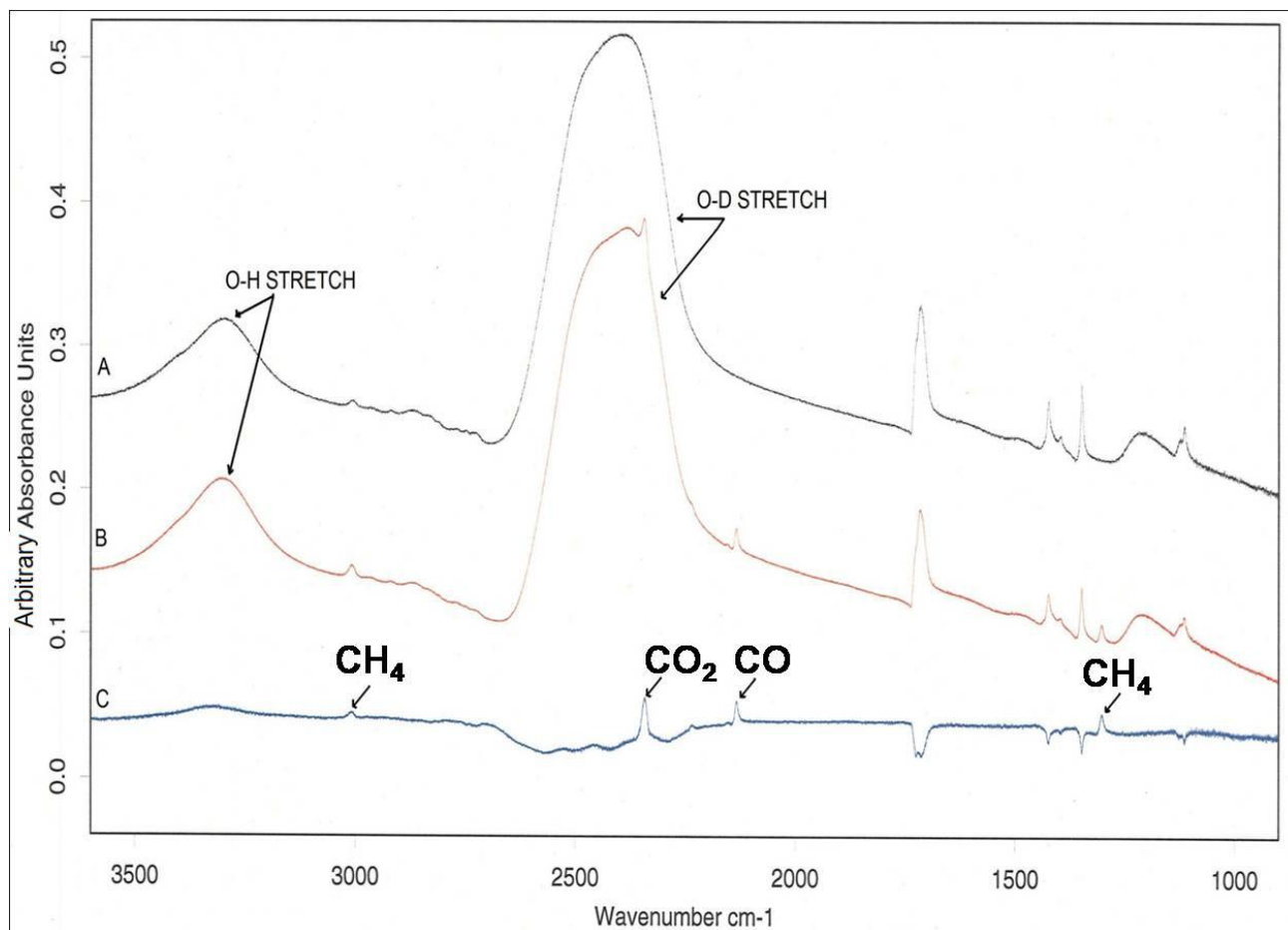
Fig. 41 IR Spectra of CH_3CHO trapped in D_2O ice at T = 14 K (ratio: 1/11)   **A.** After deposition
B. After 630min irradiation   **C.** difference spectrum

IR spectra of $CD_3CDO{:}H_2O$ (1:50) at a temperature of 6K before and after 300min UV photolysis is illustrated in figure 42. The O-H stretching vibration of H_2O ice was observed around 3200-3600cm^{-1}. Absorption bands at 2341cm^{-1} and 2134cm^{-1} are assigned to CO_2 and CO respectively. A small absorption band corresponding to C-D stretching vibration of the CD_4 molecule was observed at 2250cm^{-1}. The formation of stronger hydrogen bonds results in a shift of the O-H stretching vibration to 3100cm^{-1} – 3300cm^{-1}.
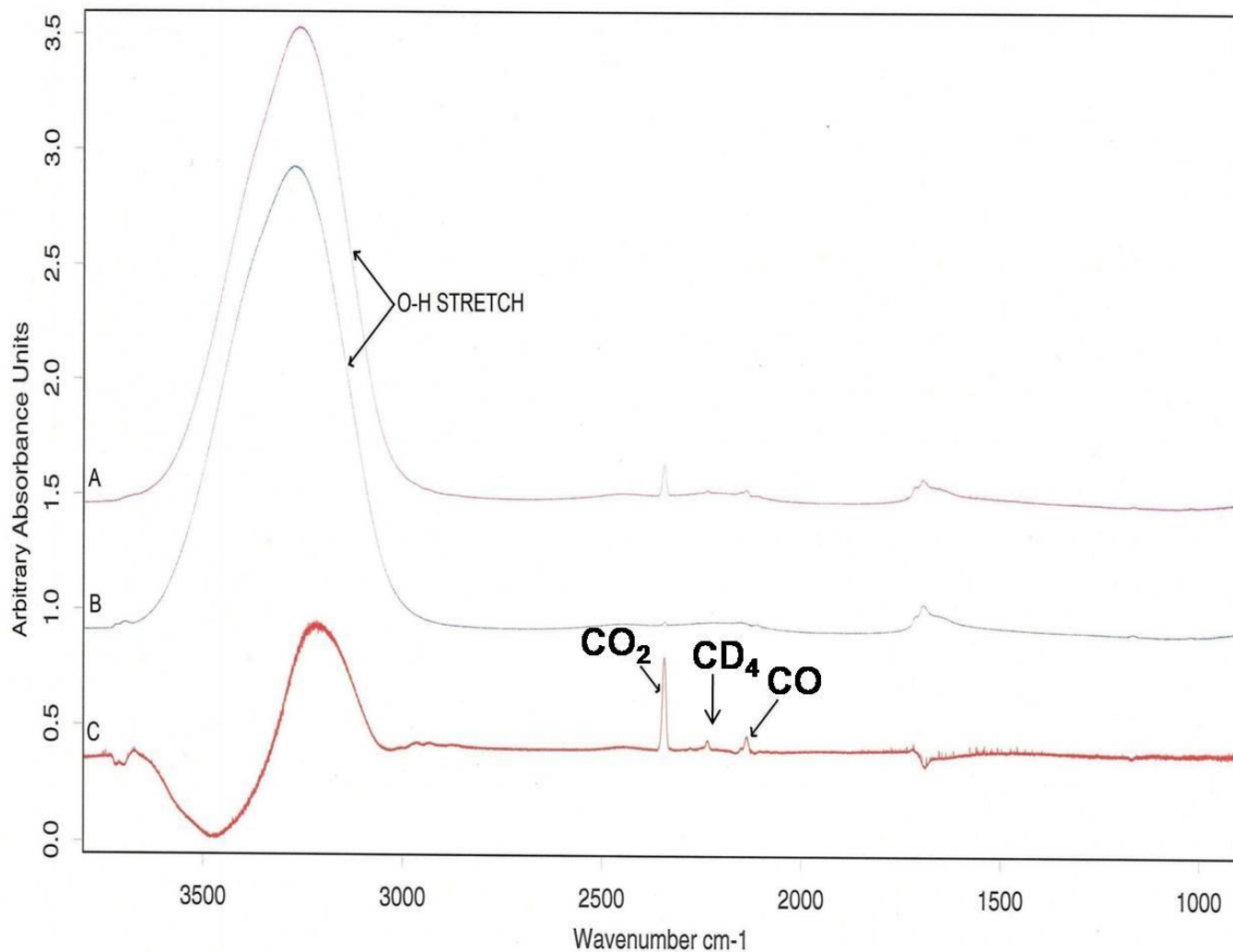
Fig.42 IR spectra of CD_3CDO trapped in H_2O ice at T= 6 K (ratio: 1/50)
A. After 300min irradiation **B.** After deposition **C.** Difference spectrum

IR spectra of $CD_3CDO:D_2O$ (1:11) recorded at a 14K before and after 730min UV irradiation are shown in figure 43. Major photoproducts observed were CO_2, CO and CD_4. Broad absorption bands at 3310cm^{-1} and 2535cm^{-1} are attributed to O-H stretching vibration and O-D stretching vibration of HDO ice, respectively. Absorption bands of CO_2 and CO were observed at 2341cm^{-1} and 2135cm^{-1}, respectively. Small absorption bands relating to C-D stretching vibration and C-D deformation modes of CD_4 appeared around 2250cm^{-1} and 995cm^{-1}, respectively.
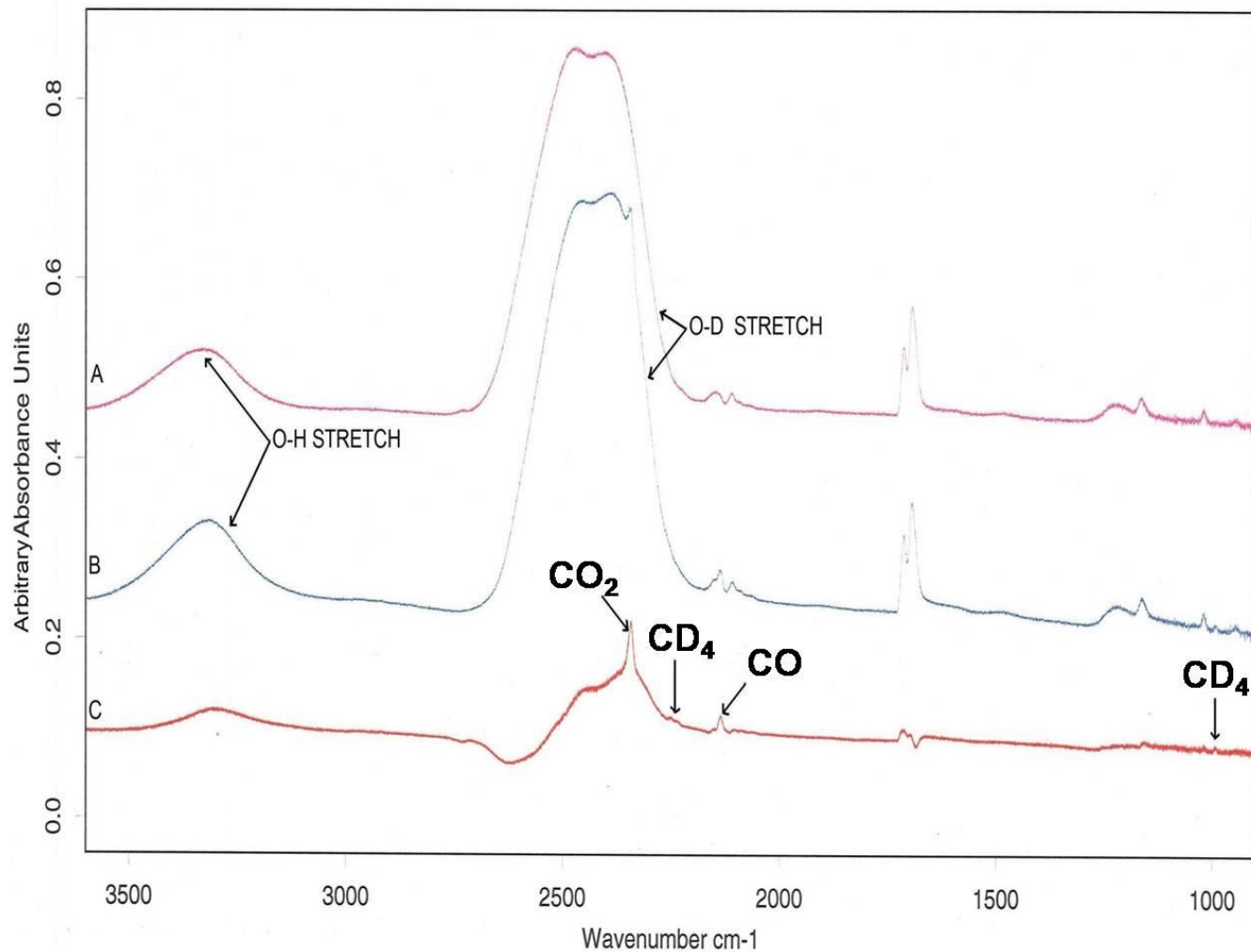
Fig.43 IR spectra of CD_3CDO trapped in D_2O ice at T = 14 K (ratio: 1/11) **A.** After deposition **B.** After 730min irradiation **C.** Difference spectrum

IR spectra of $CD_3CDO:H_2O:Ar$ (1:10:1000) at a temperature of 14 K before and after 405min UV irradiation is illustrated in figure 44. O-H stretching vibration of H_2O ice was observed around 3200-3600cm^{-1}. Absorption bands at 2341cm^{-1} and 2134cm^{-1} are assigned to CO_2 and CO respectively. Absorption bands corresponding to C-D stretching vibration and deformation modes of CD_4 molecule was observed at 2250cm^{-1} and 990cm^{-1}. Small absorption band assigned to isolated O-H bending vibration appeared around 1600cm^{-1}.
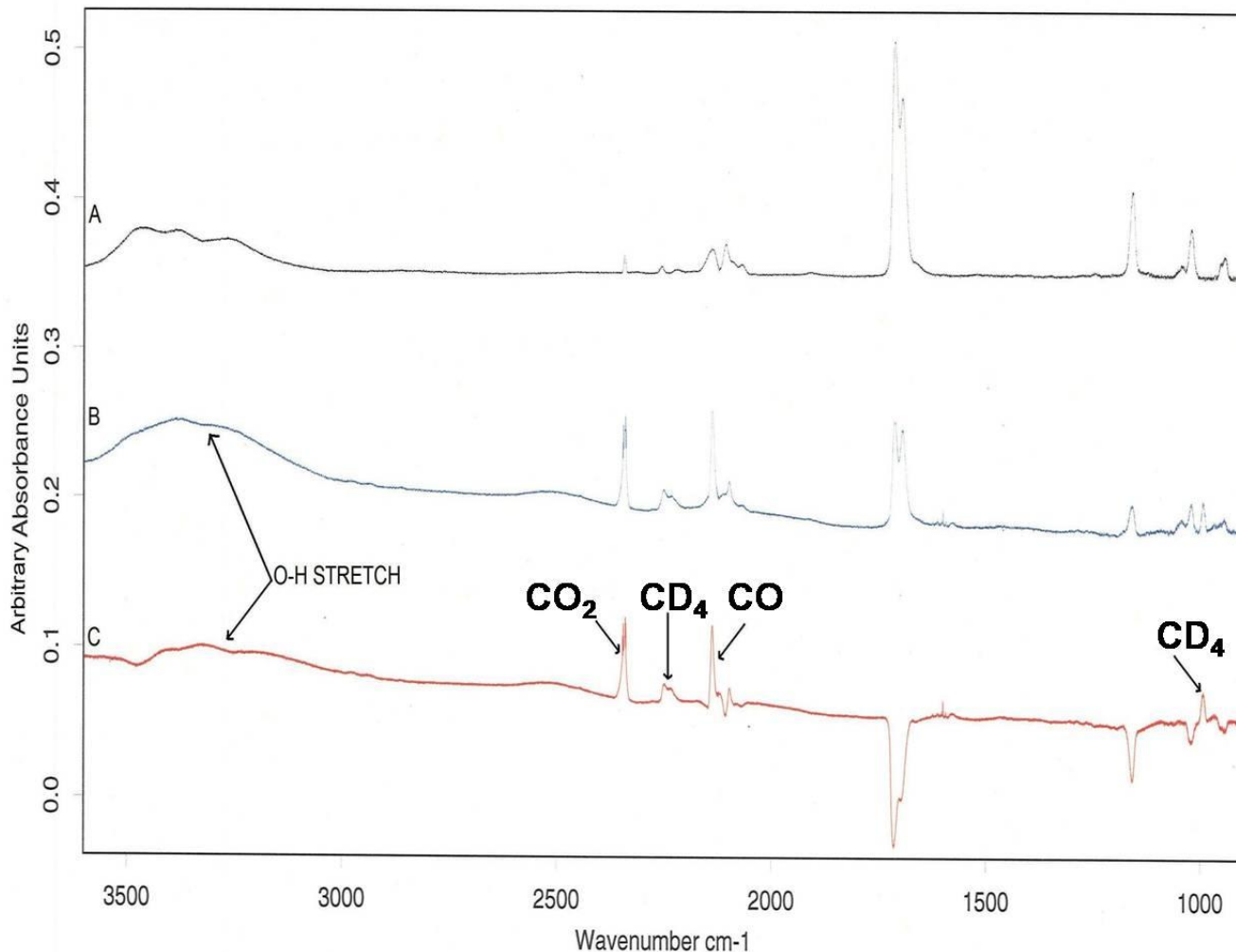
Fig.44 IR spectra of CD_3CDO trapped in H_2O ice and solid Ar at T= 14 K
A. After deposition **B.** After 405min irradiation **C.** difference spectrum

In summary, photochemical decomposition of acetaldehyde in the gas phase, trapped in solid rare gases, H_2O ice and D_2O ice was observed. Photoproducts from the series of experiments conducted were CO_2, CO, H_2O, CH_4 and CD_4.

3.4.2 Acrylic acid ($CH_2CHCOOH$)

IR spectra of $CH_2CHCOOH$:Ar (1:1000) and $CH_2CHCOOH$:H_2O ice (1:30) at a temperature of 6 K and 14 K, respectively, were recorded. Table 7 shows the assigned fundamental vibrations of $CH_2CHCOOH$ trapped in these matrices. Assignments were based on

the works of **A.Kulbida et. al [25], M.Orgill et. al [24] and S.W.Charles et al [61].** Many of the absorption bands of $CH_2CHCOOH$ trapped in solid argon were observed to be close doublets, indicating the formation of dimers as well as the presence of conformational isomers as mentioned in section 3.2.2.

IR spectra of pure $CH_2CHCOOH$ before and after irradiation was recorded at a temperature of 14 K (see fig 45). Photoproducts observed were mainly CO_2 and CO. Traces of $^{13}CO_2$ also appeared. A "free O-H" absorption band was also observed around $3600cm^{-1}$.
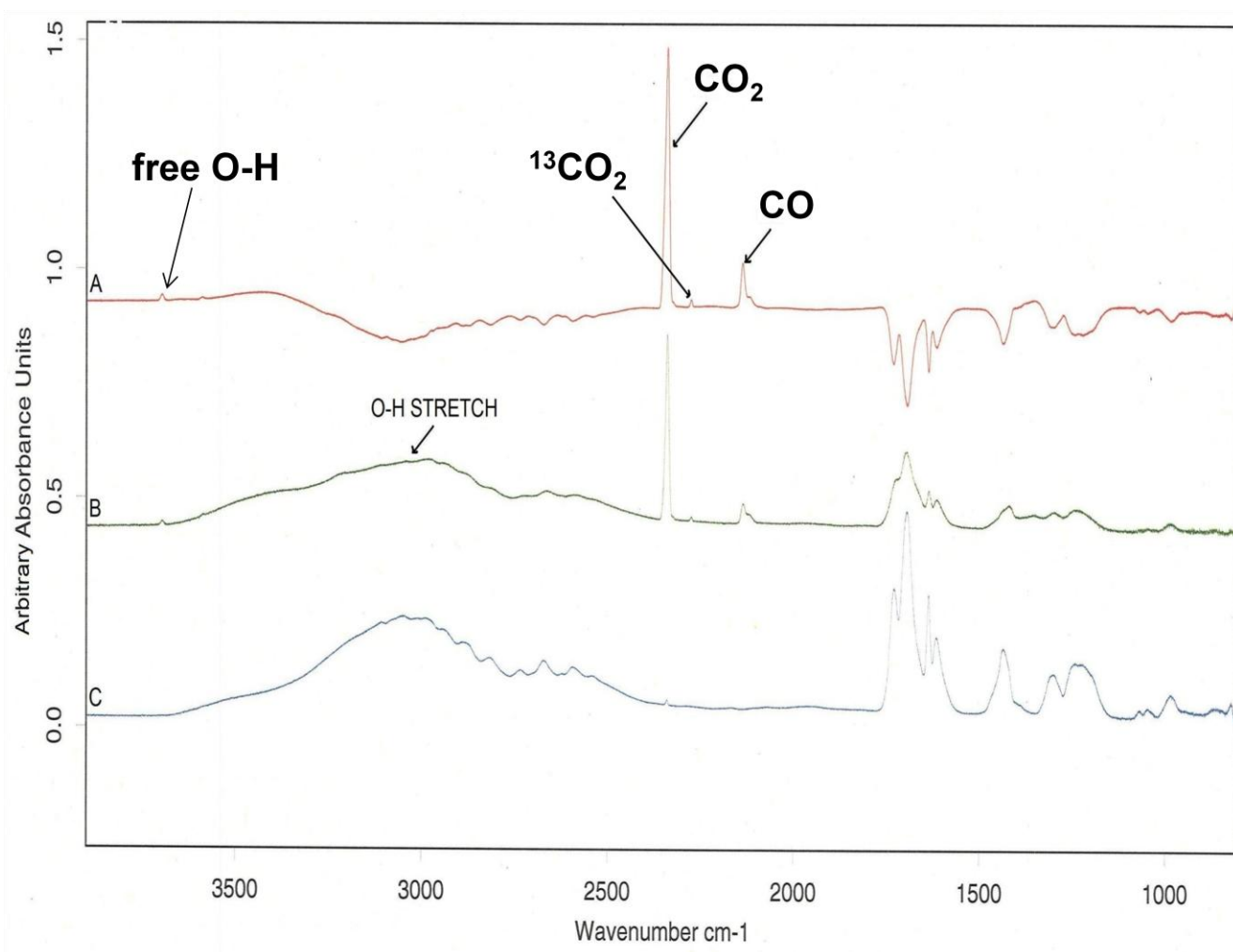
Fig. 45 IR spectra of pure $CH_2CHCOOH$ at T = 14 K **A.** Difference spectrum after 70min irradiation **B.** After 40min irradiation **C.** After deposition

CH₂CHCOOH:Ar (cm⁻¹)	CH₂CHCOOH:H₂O ice (cm⁻¹)	Assignments
3711	3000-3700	υ (O-H)
3571	-	υ (O-H)
3532	-	υ (O-H)
2770	2726	υ (CH₂)$_{as}$
2700	2655	υ (C-H)
2603	2582	υ (CH₂)$_s$
1782	1684	υ (C=O)
1761	1677	υ (C=O) / δ (O-H)
1749	1639	υ (C=O) / δ (O-H)
1640	1614	υ (C=C)
1608	-	υ (C=C)
1425	1436	δ(CH₂)$_{as}$
1398	1405	δ (CH₂)$_{as}$
1306	1307	υ (C-O)+ δ(C-O-H)
1285	-	υ (C-O)+ δ(C-O-H)
1279	1249	δ(C-H)
1219	-	δ (C-H)
1206	-	δ (C-H)
1184	1154	υ (C-O)
1145	1143	υ (C-O)
1102	1125	ω(CH₂)
1062	1118	ω (C-H)
1035	-	υ (C-C)
1016	-	υ (C-C)

υ - stretching, δ – bending, ω – wagging, $_{as}$ – asymmetric, $_s$ – symmetric

Table 7: Fundamental vibrations of CH₂CHCOOH trapped in solid Argon and H₂O ice

IR spectra of $CH_2CHCOOH$ trapped in solid Argon (1:1000) before and after UV photolysis was recorded at a temperature of 6 K (see fig. 46). New absorption bands which appeared after the UV irradiation were mainly CO_2 and CO. Additional absorption bands appeared around 1711 cm^{-1} and 1207cm^{-1} which resembles C=C stretching vibration and C-H bending modes of ethylene (C_2H_4) respectively. This assignment cannot be confirmed precisely, hence further studies need to be conducted.
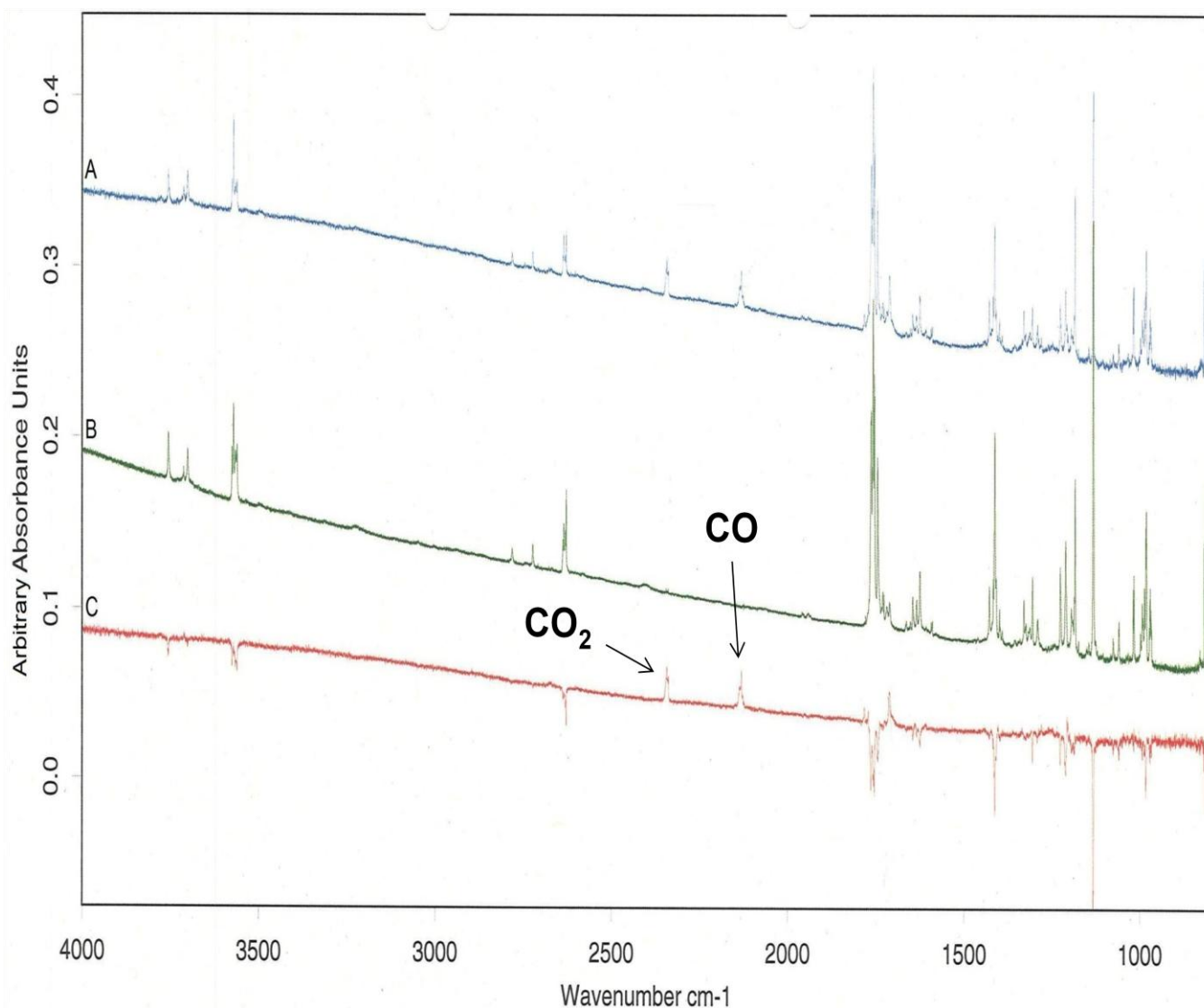
Fig. 46 IR spectra of $CH_2CHCOOH$ trapped in solid Ar at T = 14 K
A. After 300min irradiation **B.** After deposition **C.** Difference spectrum

The last experiment was the investigation of $CH_2CHCOOH$ trapped in H_2O ice at a temperature of 14 K (see fig 47). Photoproducts observed after UV irradiations were CO_2 and CO. Traces of $^{13}CO_2$ appeared around 2280cm^{-1}. The O-H stretch of H_2O ice was also observed around 3000 – 3500cm^{-1}.
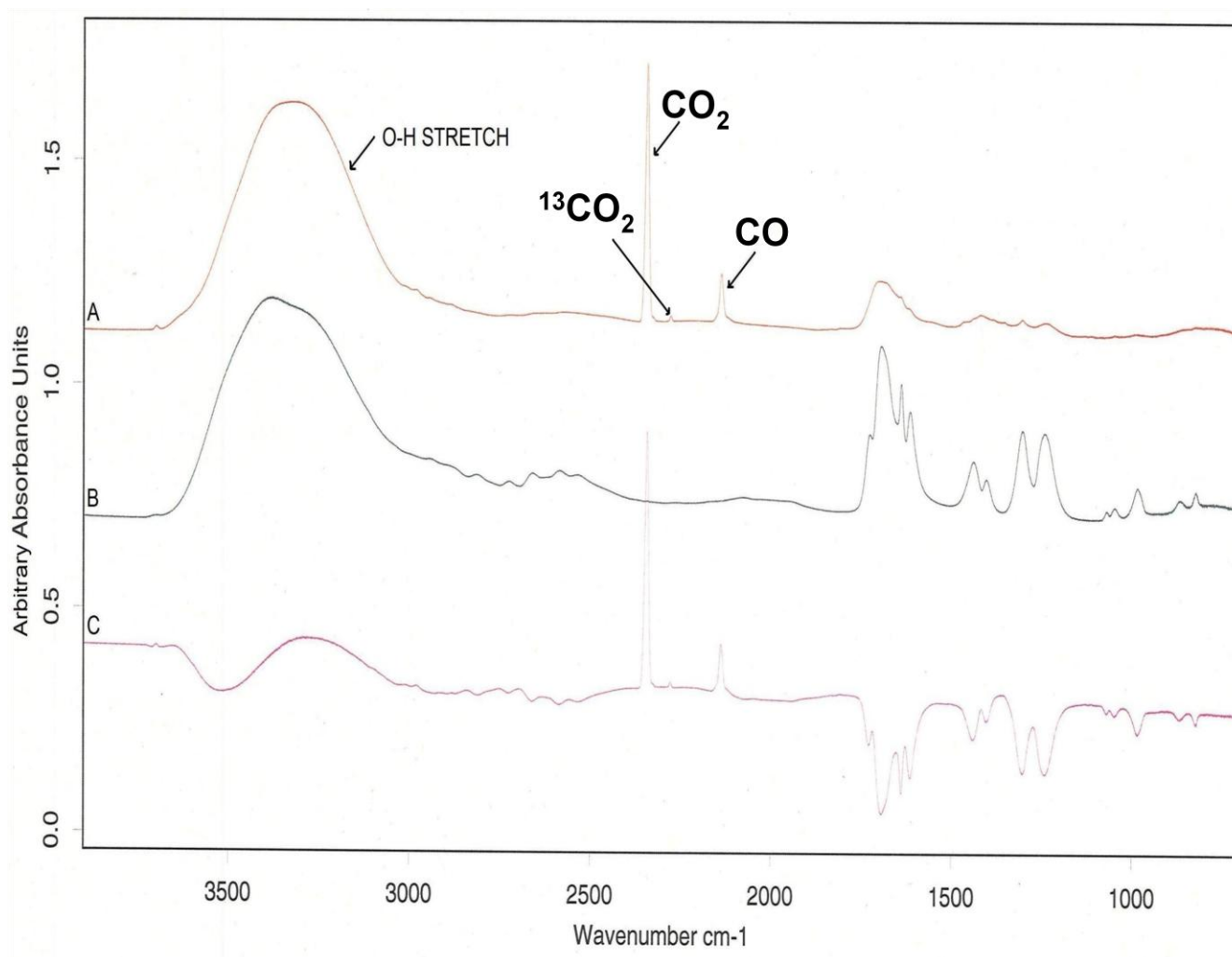
Fig. 47 IR spectra of $CH_2CHCOOH$ trapped in H_2O ice at T= 14 K (ratio: 1/ 10)
A. After 240min irradiation **B.** After deposition **C.** Difference spectrum

In summary, photodissociation of $CH_2CHCOOH$ trapped in solid Argon and H_2O ice resulted in the formation of new molecules notably, CO_2 and CO.

Chapter 4: Summary and Conclusions

Studies on snowpack have come to a conclusion that, snowpack is a multiphase reactor in which physical exchange processes, heterogeneous reactions and photochemical reactions take place. Snowpack processes and atmosphere – snow gas exchange have demonstrated that, chemical and physical interactions between the snowpack and the overlying atmosphere have a substantial impact on the composition and/or chemistry of the overlying atmosphere. It is increasingly recognized that photochemical reactions of compounds in snow have important implications for the composition of the atmospheric boundary layer in snow - covered regions and for the interpretation of concentration profiles in snow and ice regarding the composition of the past atmosphere. **[11]**

In this work, cryogenic spectroscopy techniques have been applied to study the photochemical decomposition of two atmospheric pollutants (carbonyl compounds) trapped in solid rare gases and H_2O ice. Photoproducts observed after UV photolysis of acetaldehyde and acrylic acid were:

CH_3CHO $\qquad\qquad\qquad$ $CH_2CHCOOH$

Gas phase	Rare gases	H_2O ice		Rare gas	H_2O ice
CO	CO	CO		CO	CO
CH_4	CH_4	CH_4		CO_2	CO_2
CO_2	CO_2	CO_2		C_2H_4 (?)	-
H_2O	-	-		-	-

Table 8. Photoproducts of CH_3CHO and $CH_2CHCOOH$ after UV photolysis

Laboratory studies of snow/ice photochemistry can deliver important contributions to describe the true processes in ice and on ice surfaces in the "real nature" because the physical and

chemical nature of the surface of snow and ice is not well understood. However, so far it is not clear what effect ionic species contained in snow have on ice surface structure, composition and chemistry. The quasi liquid layers (QLL) which affect or change the way molecules stick to the surface of ice (adsorption onto or dissolution into the QLL) are not observed in our laboratory snow/ice photochemistry experiments due to the low temperatures applied. In order to relate this study to atmospheric conditions, several features must be considered: for instance, secondary reactions are often prevented and also the 'cage effect' can alter the relative efficiencies of expected reaction pathways. **[50]**

Laboratory studies of snow/ice photochemistry provide further information of photochemically generated trace gases and their subsequent release into the overlying atmosphere. It helps to develop computer models which mimic the chemistry at the ice/atmosphere interface. Photochemistry in snowpack may remove organic molecules and produce small molecules (e.g. CO, CO_2, etc.) as demonstrated in this work. The CO_2 and CO molecules produced in snowpack photochemistry could affect CO_2 records especially in Greenland ice cores where there are much more organics deposited than in Antarctica.

References

1. **V. F. McNeill and M. G. Hastings,** "Ice in the environment: connection to atmospheric chemistry" Environmental Research Letters, 3, 045004, 1pp (2008)

2. **A. M. Grannas, A. E. Jones, J. Dibb et al.,** "An overview of snow photochemistry: evidence, mechanisms and impacts" Atmospheric chemistry and physics, 7, 4329–4373 (2007)

3. **D. Helmig, L. Ganzeveld, T. Butler and S. J. Oltmans** "The role of ozone atmosphere-snow gas exchange on polar, boundary-layer tropospheric ozone – a review and sensitivity analysis" Atmospheric chemistry and physics 7, 15 – 30, (2007)

4. **Prof. Dr. Peter Lemke** "Climate I, lectures notes, SS 2009", Postgraduate   Environmental Physics (PEP),University of Bremen.

5. **A.P.M Baede, E. Ahlonsou, Y. Ding, D. Schimel, B. Bolin, S. Pollonais** " The climate system: an overview. In: Climate Change 2001: The scientific Basis. Contribution of working group I to the third Assesment Report of the IPCC, [J.T. Houghton, Y. Ding, D.J. Griggs, M. Noguer, P.J. van der Linder, X. Dai, K. Maskell and C.A. Johnson (eds)]" Cambridge university press, Cambridge, UK and New York, NY, USA, 82pp.

6. **Prof. Dr. Otto Schrems** "Atmospheric chemistry II, Lecture notes, SS 2009", Postgraduate Environmental Physics (PEP), University of Bremen.

7. **Weblink: http://** www.kidsgeo.com/images/atmosphere-temperature.jpg

8. **Weblink: http:**//www1.lsbu.ac.uk/water/ice1h.html

9. **Weblink:** www.practicalchemistry.org/data/images/originals/the-density-of-ice-187.jpg

10. **T. Huthwelker, M. Ammann and T. Peter**, "The uptake of acidic gases on ice" Chemical Reviews, Volume 106, No.4, 1375-1444 (2006)

11. **F. Domine and P. B. Shepson** "Air-snow interactions and atmospheric chemistry" Science, Vol. 297, No.5586, 1506-1510 (2002)

12. **P. Klan and I. Holoubek** "Ice (photo) chemistry. Ice as a medium for long-term (photo) chemical transformation – environmental implications" Chemosphere 46, 1201 – 1210, (2002)

13. **J. Cyriac and T. Pradeep,** "Structural transformation in formic acid on ultra cold ice surfaces" Chemical Physics Letters 402, 116-120 (2005)

14. **A. Schriver, J. M. Coanga, L. Schriver-Mazzuoli and P. Ehrenfreund,** " FTIR studies of ultraviolet photo-dissociation at 10K of dimethyl ether in argon and nitrogen matrices,in

the solid phase and in amorphous water ice", Chemical Physics Letters 386, 377-383 (2004)

15. **P.K. Hudson, M.A. Zondlo and M. A. Tolbert**, "The interaction of methanol, acetone and acetaldehyde with ice and nitric acid-doped ice: Implications for Cirrus Clouds" Journal of Physical Chemistry. A, 106 (12), 2882-2888 (2002)

16. **P. S. Liss, A. D. Hatton, G. Malin, P.D. Nightingale and S. M. Turner,** "Marine Sulphur emissions" Philosophical transactions of the Royal Society B., 352(1350), 159-169 (1997)

17. **C.O.Della Vedona and O.Sella**, "Raman and Infrared spectra and Photochemical behavior of acetaldehyde isolated in matrices" Journal of Raman spectroscopy, Vol.22, 505-507 (1991)

18. **M. Petitjean, Ph. Mirabel and S. Le Calvé,** "Uptake Measurements of Acetaldehyde on Solid Ice Surfaces and on Solid/Liquid Supercooled Mixtures Doped with HNO_3 in the Temperature Range 203−253 K", Journal of Physical Chemistry. A, 113 (17), pp 5091–5098, (2009)

19. **S. Houdier, S. Perrier, F. Dominé, A. Cabanes, L. Legagneux, A. M. Grannas, C. Guimbaud, P. B. Shepson, H. Boudries and J. W. Bottenheim**, "Acetaldehyde and acetone in the Arctic snowpack during the ALERT2000 campaign. Snowpack composition, incorporation processes and atmospheric impact", Atmospheric Environment, Vol. 36, Issues 15-16, pp 2609-2618, (2002)

20. **C. Guimbaud, A.M. Grannas, P. B. Shepson, J.D. Fuentes, H. Boudries, J. W. Bottenheim, F.Dominé,   S. Houdier, S. Perrier, T. B. Biesenthal and B. G. Splawn**, "Snowpack processing of acetaldehyde and acetone in the Arctic atmospheric boundary layer**"** Atmospheric Environment, Vol. 36, Issues 15-16, pp 2743-2752,(2002)

21. **F. Domine, S. Houdier, A.-S. Taillandier and W. R. Simpson**, "Acetaldehyde in the Alaskan subarctic snowpack", Atmospheric Chemistry and Physics, 10, pp 919–929, (2010)

22. **D. B. Millet, A. Guenther, D. A. Siegel, N. B. Nelson, H. B. Singh, J. A. de Gouw, C. Warneke, J. Williams, G. Eerdekens, V. Sinha, T. Karl, F. Flocke, E. Apel, D. D. Riemer, P. I. Palmer, and M. Barkley** "Global atmospheric budget of acetaldehyde: 3-D model analysis and constraints from in-situ and satellite observation", Atmospheric Chemistry and Physics, 10, 3405-3425, (2010).

23. **J.Umemura and S.Hayashi,** "Infrared Spectra and Molecular Configurations of Liquid and Crystalline Acrylic Acids", Bulletin of the Institute for Chemical Research, Kyoto University, 52(4): 585-595, (1974)

24. **M. Orgill, B. L. Baker and N. L. Owen** "FTIR studies of conformational isomerism in acrylates and acrylic acids", Spectrochimica Acta, Part A, Vol. 55, 1021-1024, (1999)

25. **A.Kulbida, M. N. Ramos, M. Rasanen, J. Nieminen, O. Schrems and R. Fausto "Rotational isomerism in acrylic acid. A combined matrix-isolated IR, Raman and ab initio molecular orbital study",** Journal of the chemical society, Faraday transaction articles, Vol. 91(11), 1571-1585, (1995)

26. **B.Weiner and R. N. Rosenfield, "**Photofragmentation of Acrylic Acid and Methacrylic Acid in the Gas Phase**",** Journal of the American Chemical Society, 105, pp 6233-6236, (1983)

27. **M.C. Osborne, Q. Li and I.W. M. Smith** "Products of the ultraviolet photodissociation of trifluoroacetic acid and acrylic acid", The Journal of physical chemistry and The Journal of chemical physics, Vol.1, 1447-1454, (1999)

28. **Wei-Hai Fang and Ruo-Zhuang Liu**, "Photodissociation of Acrylic Acid in the Gas Phase: An ab Initio Study", Journal of the American Chemical Society, 122 (44), pp 10886–10894, (2000)

29. **Weblink:http://**www.scipp.ucsc.edu/~haben/archives/physics5B08/Electromagentic-spectrum-3.png

30. **Weblink: http://**www.orgchem.colorado.edu/hndbksupport/irtutor/tutorial.html

31. **Ronald Macatangay and Janina Messerschmidt,** "Fourier Transform Infrared Spectroscopy Laboratory Manual SS 2009", Postgraduate Environmental Physics, University of Bremen.

32. **Dr. Björn-Martin Sinnhuber,** "Remote Sensing Lecture notes SS 2009". Postgraduate Environmental Physics (PEP), University of Bremen.

33. **C.N. Banwell and E.M. McCash,** "Fundamentals of Molecular Spectroscopy", 4th edition, McGraw-Hill Companies, pg 55-99, (1994).

34. **B.Stuart,** "Infrared Spectroscopy: Fundamentals and Applications", John Wiley and Sons Ltd, New York, (2004).

35. **Weblink: http:**//wwwchem.csustan.edu/Tutorials/infrared.htm

36. **G. Herzberg**, "Infrared and Raman Spectra of Polyatomic Molecules", Van Nostrand Reinhold, New York NY, (1945).

37. R. Eisberg and R. Resnick, "Quantum Physics of Atoms, Molecules, Solids, Nuclei and Particles", 2nd edition, John Wiley and Sons, New York, (1985).

38. Weblink: http://www.le.ac.uk/ch/pdf/teachersworkshops.pdf

39. Weblink:http://www.atu.edu/chemistry/people/anwar/Course/Chem%204414/Chapter%2016.ppt

40. Michael Bradley "Advantages of a Fourier Transform Spectrometer" Thermo Fisher Scientific, Technical note: 50674, Madison, WI,USA, (2008)

41. Weblink: http://members.xoom.it/alberto_chim/ir%20ABSORBITION.doc

42. Weblink: http:// www2.ups.edu/faculty/hanson/Spectroscopy/IR/IRfrequencies.html

43. Weblink: http://www.scitopics.com/Matrix_Isolation.html

44. S. Cradock and A. J. Hinchcliffe, "Matrix isolation-A technique for the study of reactive inorganic species", Cambridge University Press, pp 1-3 (1975)

45. Bruker IFS 66v Working manual, http://www.brukeroptics.com/ftir.html

46. T. Shiraishi, Y. Soma, O. Ishitani and K. Sakamoto, "Application of an integrated PrepStation-GC-NPD system to automated continuous measurement of formaldehyde and acetaldehyde in the atmosphere" Journal of environmental monitoring, 3,654-660 (2001)

47. D. Grosjean, A. H. Miguel and T. M. Tavares, "Urban air pollution in Brazil: acetaldehyde and other carbonyls" Atmospheric environment, Vol. 24B, No.1, pp 101-106 (1990)

48. Weblink:http://www.biochem.arizona.edu/classes/bioc462/462bh2008/462bhonorsprojects/462bhonors2006/lowej/Acetaldehyde/acetaldehyde.png

49. L. Benning and A. Wahner, "Measurements of atmospheric formaldehyde (HCHO) and acetaldehyde (CH_3CHO) during POPCORN 1994 using 2.4-DNPH coated silica cartridges" Journal of Atmospheric Chemistry 31: 105-117 (1998)

50. J.R.Sodeau "The photolysis and photo-oxidation of simple aliphatic aldehydes in low temperature matrices", Spectrochimica Acta. Vol. 46A, No. 6,887-901, (1990)

51. A.Horowltz and J.G.Calvert "Wavelength dependence of the primary processes in acetaldehyde photolysis", The Journal of physical chemistry, Vol.86, No.16, (1982)

52. **E. J. K. Nilsson, L. Bache-Andreassen, M. S. Johnson and C. J. Nielsen**, "Relative tropospheric photolysis rates of acetaldehyde and formaldehyde isotopologues measured at the European photoreactor facility", The Journal of physical chemistry, Vol.113, No.15, 3498-3504, (2009)

53. . **H.A.Cruse and T.P.Softley** "Velocity-map imaging study of the photodissociation of acetaldehyde", The Journal of chemical physics, Vol.122, 124303, (2005)

54. **S.Chen and W.H. Fang** "Insights into photodissociation dynamics of acetaldehyde from ab initio calculations and molecular dynamics simulations", The Journal of chemical physics, Vol.131, 054306, (2009)

55. **W.Schneider and G.K. Moortgat**, Private Communication, MPI, Mainz, (1989)

56. **Weblink:** http://upload.wikimedia.org

57. **Weblink:** http://www.assembly.ab.ca/lao/library/egovdocs/alen/2002/140570.pdf

58. **D. C. Kitchen, N. R. Forde, and L. J. Butler** "Photodissociation of acrylic acid at 198 nm", The Journal of physical chemistry, Vol. 101, 6603-6610, (1997)

59. **T. Shimanouchi**, "Tables of Molecular Vibrational Frequencies Consolidated Volume I", National Bureau of Standards, 1-160 (1972)

60. **H. Zhao, J.Kim and B.E. Koel**, "Adsorption and reaction of acetaldehyde on pt(111) and Sn/PT(111) surface alloys" Surface Science 538, 147–159 (2003)

61. **S. W. Charles, F. C. Cullen, N. L. Owen and G. A. Williams** "Infrared spectrum and rotational isomerism of acrylic acid", Journal of molecular structure, Vol. 157, 17-29, (1987)